Proc Natl Acad Sci USA: doi: 10.1073/pnas.2024562118

MK2 degradation as a sensor of signal intensity that controls stress-induced cell fate

Nuria Gutierrez-Prat[a,1,2], Monica Cubillos-Rojas[a,1], Begoña Cánovas[a,1], Antonija Kuzmanic[b], Jalaj Gupta[a,2], Ana Igea[a,2], Elisabet Llonch[a], Matthias Gaestel[c], and Angel R. Nebreda[a,d,3]

[a] Institute for Research in Biomedicine (IRB Barcelona), The Barcelona Institute of Science and Technology, 08028 Barcelona, Spain

[b] University College London, Gower Street, London WC1E 6BT, UK

[c] Institute of Cell Biochemistry, Hannover Medical School, Carl-Neuberg-Str.1 30625 Hannover, Germany

[d] ICREA, Pg. Lluís Companys 23, 08010 Barcelona, Spain

[1] These authors contributed equally

[2] Present addresses: F. Hoffmann-La Roche, 4070 Basel, Switzerland (N.G.-P.); Sanjay Gandhi Post Graduate Institute of Medical Sciences, 226014 Lucknow, Uttar Pradesh, India (J.G.); Fundación Instituto de Investigación Sanitaria de Santiago de Compostela, Spain (A.I.)

[3] Correspondence: angel.nebreda@irbbarcelona.org, Phone +34- 934031379

Running title: MK2 levels modulate the stress response

Keywords: stress, cell survival, p38α, MK2, MDM2, activation kinetics, cell fate

NGP ORCID: 0000-0001-6717-8434
MCR ORCID: 0000-0003-2867-1773
BC ORCID: 0000-0002-2546-0295
AK ORCID: 0000-0003-2815-5605
JG ORCID: 0000-0002-0153-080X
AI ORCID: 0000-0002-6658-4518
EL ORCID: 0000-0003-3979-2597
MG ORCID: 0000-0002-4944-4652
ARN ORCID: 0000-0002-7631-4060

Abstract

Cell survival in response to stress is determined by the coordination of various signaling pathways. The kinase p38α is activated by many stresses but the intensity and duration of the signal depends on the stimuli. How different p38α activation dynamics may impact cell life/death decisions is unclear. Here, we show that the p38α signaling output in response to stress is modulated by the expression levels of the downstream kinase MK2. We demonstrate that p38α forms a complex with MK2 in non-stimulated mammalian cells. Upon pathway activation, p38α phosphorylates MK2, the complex dissociates and MK2 is degraded. Interestingly, transient p38α activation allows MK2 re-expression, reassembly of the p38α-MK2 complex and cell survival. In contrast, sustained p38α activation induced by severe stress interferes with p38α-MK2 interaction resulting in irreversible MK2 loss and cell death. MK2 degradation is mediated by the E3 ubiquitin ligase MDM2, and we identify four lysine residues in MK2 that are directly ubiquitinated by MDM2. Expression of a MK2 mutant that cannot be ubiquitinated by MDM2 enhances the survival of stressed cells. Our results indicate that MK2 re-expression and binding to p38α is critical for cell viability in response to stress, and illustrate how particular p38α activation patterns induced by different signals shape the stress-induced cell fate.

Significance

In response to stress, cells can activate several mechanisms that support functionality and survival. However, strong or persistent stresses usually trigger a deleterious answer that leads to cell death. The protein kinases p38α and MK2 are implicated in a stress signaling pathway. Here we characterize a molecular mechanism that helps to translate the stress-induced activation of the p38α-MK2 pathway into appropriate biological responses. We show that MK2 expression levels are regulated by the stress intensity, and that degradation of MK2 triggered by ubiquitination is linked to cell death. This mechanism will be valuable to better understand the implication of this signaling pathway in pathologies such as inflammatory diseases and cancer.

INTRODUCTION

Cells can respond to stress in a variety of ways through the activation of particular signaling pathways. The initial response is usually aimed at protecting the cell against the insult to facilitate damage recovery and cell survival. However, if the harmful stimulus persists or is not properly resolved, a death program is usually activated that eventually eliminates the damaged cells.

A signaling pathway that is frequently associated with the stress response involves activation of the mitogen-activated protein kinase (MAPK) family member p38α. Upon activation, generally achieved by dedicated MAP2Ks, p38α can phosphorylate a variety of substrates in the nucleus and cytoplasm (1, 2). In particular, the activation of p38α is often linked to the activation of MAPK-activated protein kinase 2 (MAPKAPK2 or MK2), and both kinases regulate several stress responses that impinge on cell survival or cell death (3-6). In addition, the p38α-MK2 pathway plays an important role in the regulation of the immune response, and it can also control the proliferation or differentiation of some cell types, which may contribute to physiological responses not necessarily related to stress (7-9). How this pathway can mediate so many different cellular processes is still largely an open question. In many cases, the cellular response mediated by the p38α-MK2 pathway can be determined by the cell type and the stimuli, and often engages particular downstream targets. However, other factors such as signaling dynamics may also play a role. It has been reported that some MAPKs can perform different functions depending on the amplitude, duration and frequency of pathway activation (10), but it is still not known whether the p38α activation dynamics could modulate the cell responses associated to different stimuli.

The formation of protein-protein complexes is important for many biological processes, including signal transduction (11, 12), and changes in their interaction dynamics are crucial for proper sensing of the environmental changes (13). Structural analysis revealed that purified recombinant p38α and MK2 proteins can interact through the p38α docking groove and the MK2 docking motif (14), and further studies addressed the requirements for the formation of the p38α-MK2 complex in vitro (15, 16). Moreover, nuclear magnetic resonance and X-ray crystallography analysis suggested that p38α-MK2 can form different heterodimers depending on the activation state of p38α (17). However, little is known on how this interaction could be regulated in vivo, and whether it modulates the pathway functions.

Given the importance of p38α and MK2 in many cellular processes, the activity of both kinases should be tightly controlled. The downregulation of p38α activity is known to involve several phosphatases and negative feedback loops (18-22). However, it is not clear how MK2 activity is normally downregulated.

In this study, we present evidence that the extent of p38α activation regulates MK2 protein levels, which in turn have a key role in the pathway output. We show that endogenous p38α and MK2 form a complex in mammalian cells, and upon p38α activation the complex dissociates and MK2 is degraded. In response to mild stress or to physiological stimuli, the pathway is transiently activated allowing re-formation of the p38α-MK2 complex and concomitant cell survival. However, cells treated with severe stress show sustained p38α activation, which interferes with p38α-MK2 interaction leading to the irreversible loss of MK2 and cell death. Therefore, our results illustrate a new mechanism of p38α-MK2 pathway regulation, which might help to predict the cell fate in response to stress.

RESULTS

Stress-induced p38α activation leads to MK2 downregulation. The p38α-MK2 pathway has been connected to several pathologies such as cancer and autoimmune diseases (23-25). Therefore, the pathway activity needs to be strictly controlled for normal physiology. Accordingly, several mechanisms have been reported to account for p38α inhibition (2, 21, 22). In contrast, and despite a well-recognized role of MK2 in the stress response (3, 4, 6), very little is known about how it becomes inactivated. To address this, we monitored the MK2 activation kinetics in cells treated with stress-inducing agents by analyzing two different phosphorylation sites. It should be noted that endogenous MK2 can be expressed as two different protein isoforms (26), explaining why one or two MK2 bands are observed depending on the cell line. We focused on the lower MK2 band (shorter isoform), because it is ubiquitously expressed in cell lines. We found that the ultraviolet-light (UV) and anisomycin induced phosphorylation of p38α and MK2 unexpectedly correlated with a rapid downregulation of MK2 protein levels. As a consequence, while p38α was still phosphorylated at later timepoints, MK2 activity was shut down (Fig. 1A and 1B). This finding was reproduced in several cell lines treated with diverse stress stimuli (Fig. 1C), as well as in mouse mammary tumors treated with osmotic stress (Fig. 1D), suggesting that

downregulation of MK2 upon p38α activation is a conserved mechanism for MK2 activity inhibition in the stress response.

MK2 levels are regulated by the extent of p38α activation. The stimuli tested in the above experiments are harmful for cells and eventually result in cell death. However, p38α and MK2 are known to be activated also in physiological situations that do not necessarily lead to cell death, such as cytokine production in immune cells or during cell differentiation (7, 27, 28). To analyze the behavior of MK2 in these scenarios, we stimulated bone marrow-derived macrophages (BMDM) with lipopolysaccharide (LPS). We observed that the phosphorylation of p38α and MK2 correlated with the downregulation of MK2 protein levels at early time points. As LPS induced transient pathway activation, p38α was dephosphorylated at later time points. Strikingly, this correlated with the eventual recovery of MK2 protein levels, which was associated with increased levels of MK2 mRNA (Fig. 2A and 2B). A similar pattern was found in cancer associated fibroblasts (CAFs) incubated with transforming growth factor (TGF)-β, a signal that activates the p38α pathway and influences several processes involved in cell proliferation and differentiation (Fig. 2C and 2D). Altogether, we observed that p38α activation, either in response to stress (anisomycin, UV or H_2O_2) or to physiological stimuli (LPS and TGFβ), led to MK2 phosphorylation and the concomitant downregulation of the MK2 protein. However, when the pathway is transiently activated, MK2 levels are eventually restored, which correlates with the cells recovering the homeostatic state. Thus, the different behavior of MK2 following activation, suggests a potential link between MK2 dynamics and the cell fate in response to stress.

Different MK2 levels induced by p38α activation impinge on cell viability upon stress. Our results indicated that the extent of the p38α pathway activation led to distinct MK2 expression levels and cellular outcomes. Therefore, we hypothesized that MK2 could be more than a mere p38α substrate, but rather a modulator of the pathway output. To investigate this possibility, we selected UV irradiation as a stress stimulus that can activate the p38α pathway either in a transient or sustained manner depending on the dose. We found that in U2OS cells irradiated with 10 J/m^2 (UV10) p38α was transiently activated, as observed upon treatment of BMDMs with

LPS or CAFs with TGFβ, while the irradiation with 30 J/m^2 (UV30) resulted in a sustained activation of the pathway. In line with our initial observations, the MK2 protein was rapidly downregulated following p38α activation and restored after treatment with low UV, but not with the higher UV dose (Fig. 3A), thereby confirming the distinct behavior of the MK2 levels following transient and sustained activation of p38α. The two UV doses used have been linked to distinct cell outcomes (29). We confirmed that while some UV10 irradiated cells are able to re-enter the cell cycle and proliferate, cells treated with UV30 are mostly committed to die (Fig. 3B and Fig. 3C). To analyze the link between the extent of p38α activation and the consequent effects on MK2 protein levels and cell fate, we used a fluorescent reporter (p38α-KTR) (30) (Fig. S1A) to simultaneously track both p38α activity and the cellular outcome at the single cell level. These experiments showed that about half of the cells irradiated with UV10 did not activate p38α at all, explaining the lower MK2 phosphorylation detected in comparison to UV30-treated cells (Fig. 3D). Moreover, cells that initially activated p38α in a transient manner did not die during the course of the experiment, while a small fraction of cells that showed a heterogeneous activation pattern died. In contrast, most of the UV30 irradiated cells showed a fast and sustained p38α activation, and they all ended up dying (Fig. 3D and Fig. S1B). It should be noted that a large proportion of the UV30 irradiated cells that survived more than 15 h either never or just transiently activated p38α, and these are likely the cells that are able to proliferate and form colonies at late timepoints. Altogether, these results establish a connection between the extent of p38α activation, the MK2 protein levels and the cellular outcome.

To further support the connection between MK2 expression levels and the restoration of cellular homeostasis following stress, we analyzed the live and dead cell populations after 24 h of UV irradiation (Fig. 3E and 3F). We detected MK2 expression only in the live fraction of UV10 treated cells, corresponding to cells that eventually restore homeostasis and survive. Strikingly, MK2 was not only depleted in all dead cells, independently of the UV dose received, but also in the fraction of UV30 irradiated cells that were alive. This suggests that MK2 is degraded in cells that are subjected to an irreversible damage and are meant to die (Fig. 3F). Similar results were observed in cells treated with the chemotherapy drug cisplatin, which can activate the p38α pathway to different extents in a concentration dependent manner (Fig. S1C-1E). Altogether, our results support that MK2 protein levels are associated with the stress-induced cell fate. Thus,

mild stress induces transient activation of the p38α pathway and transient downregulation of MK2, whose levels are eventually recovered allowing the cell to function normally again. However, if the stress persists, p38α activation is sustained leading to an irreversible MK2 loss that generally results in cell death.

Impaired p38α binding results in MK2 downregulation after pathway activation. Structural analysis have shown that purified p38α and MK2 proteins can form a complex (14). To further characterize the significance of the p38α-MK2 complex, we initially confirmed that MK2 and p38α co-immunoprecipitated in lysates from cell lines and mouse tissues, indicating that the endogenous proteins are indeed associated in vivo (Fig. 4A and 4B).

Studies using recombinant proteins or based on the fission yeast homologs Sty1 and Srk1 have shown that phosphorylation reduces the binding affinities of the two proteins (31, 32). These observations led us to hypothesize that the phosphorylation of p38α and MK2 upon pathway activation could disrupt the complex, which in turn would result in reduced protein stability and the loss of MK2. To address this, we treated cells with UV to activate the pathway and then immunoprecipitated MK2. We confirmed that the MK2 protein remaining in irradiated cells was not able to bind p38α (Fig. 4C). These results were confirmed using sucrose gradients, which showed the co-localization of p38α and MK2 in the same fraction from non-stimulated cells. However, in UV irradiated cells, the co-localization was lost, MK2 levels decreased and p38α shifted towards lower molecular weight fractions, indicating that the complex dissociates and both p38α and MK2 become free (Fig. 4D). These results support that p38α pathway activation results in the separation of the p38α-MK2 complex.

The impact of complex dissociation on MK2 protein stability was further investigated using cycloheximide (CHX) to block protein synthesis. Given that exposure to CHX induces rapid p38α activation (33) and therefore separation of the p38α-MK2 complex, cells were treated with a chemical inhibitor of p38α to avoid MK2 phosphorylation and preserve the complex. We found that while p38α levels were stable independently of the complex status, the half-life of free MK2 was reduced compared to that of MK2 in complex with p38α (Fig. 4E). These observations suggest that p38α pathway activation results in complex separation and the rapid degradation of MK2, which may constitute a regulatory mechanism to shut down its kinase activity.

To corroborate these results, we analyzed the behavior of MK2 in a p38α knockout (KO) background, where complex cannot form. As expected, we observed that MK2 protein levels were decreased in p38α KO cells, and sucrose gradient analysis indicated that the MK2 remaining in these cells appeared in lower density fractions compared to WT cells (Fig. 4F). This confirms that the MK2 protein is less stable when it is not bound to p38α, either due to complex dissociation upon pathway activation or due to the absence of p38α. Accordingly, we found a severe downregulation of MK2 in p38α KO inducible systems, both in vitro and in vivo (Fig. S2A and 2B), which is consistent with studies showing reduced MK2 levels in cells derived from constitutive p38α KO embryos (34). Interestingly, the MK2 mRNA levels were similar in WT and p38α KO cells (Fig. S2C), supporting the idea that protein stability modulation plays an important role in the regulation of MK2 expression levels. Moreover, the fact that MK2 is downregulated in p38α KO cells and tissues supports a key role for p38α in the regulation of MK2 stability, and suggest a minor contribution for other p38 MAPK family members in controlling MK2 levels.

To further characterize the regulation of MK2 degradation, the p38α KO cells were reconstituted with p38α WT or several mutants. Interestingly, all the p38α mutants were able to recover the MK2 levels in p38α KO cells except the mutant with an impaired common docking (CD) site (Fig. S3), which is essential for the interactions of p38α with several regulators and substrates including MK2. These results highlight the importance of the interaction with p38α for MK2 stability. Moreover, we extended this study and stimulated with UV p38α KO cells reconstituted either with p38α WT or with p38α mutants affecting its kinase domain or the activation loop phosphorylation (35). We found that cells expressing p38α mutants with impaired kinase activity, which cannot phosphorylate MK2, were unable to downregulate MK2 expression as efficiently as the cells expressing p38α WT (Fig. 4G), suggesting that MK2 phosphorylation is required for its downregulation.

Taken together, our results indicate that p38α and MK2 form a complex in homeostasis, and stress-induced activation of both kinases results in complex disruption. If stress persists, the phosphorylated MK2 is unable to re-assemble the complex and is degraded.

MK2 released from p38α has reduced stability and is degraded by the proteasome. In eukaryotic cells, protein degradation is usually regulated by two processes: autophagy and the ubiquitin-proteasome system (36). To address how the free MK2 protein unbound to p38α is degraded, we used inhibitors of both processes. We found that inhibition of the proteasome but not of autophagy prevented MK2 degradation following pathway activation (Fig. 5A). Of note, given the sustained activation of the p38α pathway upon UV irradiation, the MK2 protein that accumulates with proteasome inhibitors is phosphorylated and failed to interact with p38α (Fig. 5B), further supporting that phosphorylation impairs the binding of the two proteins, and free MK2 is rapidly degraded by the proteasome. In addition, blocking proteasome function also partially prevented the MK2 downregulation observed in p38α KO cells (Fig. 5C), as well as in another UV-treated cell line (Fig. 5D), suggesting that this mechanism of MK2 activity regulation is probably conserved.

The proteasome is a multi-subunit complex that exists in cells in two main forms, the 20S proteasome, which is the catalytic core particle, and the 26S proteasome that incorporates a 19S regulatory subunit to both ends of the 20S form. The 19S subunit contains ATPases and deubiquitinating enzymes and is involved in the recognition of the polyubiquitin chains of the substrate and its translocation to the catalytic core (37). Although most proteins rely on ubiquitination for proteasomal degradation, it has been proposed that some proteins can be degraded by the 20S proteasome in a ubiquitin-independent manner (38, 39). To dissect the proteasome-mediated degradation of MK2, we incubated UV-treated cells with inhibitors of the 20S (MG and BTZ) or 19S proteasome subunits (AP and OPA) (40, 41). As a positive control for protein degradation mediated by the 26S proteasome, we analyzed the p53 levels. We found that all the proteasome inhibitors tested induced MK2 protein accumulation in a similar way to p53 (Fig. 5E and 5F), indicating that MK2 is degraded by the 26S proteasome complex in a ubiquitin-dependent manner.

MDM2 ubiquitin ligase controls MK2 degradation. Protein ubiquitination is mainly regulated by the interaction between specific E3 ubiquitin ligases and their target substrates (42). E3 ligases catalyze the ubiquitin transfer reaction and control the binding between the E2 ubiquitin-conjugating enzyme and the substrate (43). Using a bioinformatics platform that predicts E3 ligase-substrate interactions (44), we identified MK2 as a potential substrate for SMURF1,

STUB1 and MDM2 (Fig. S4A). To validate their potential implication, we downregulated each of these E3 ligases (Fig. S4B) and then irradiated the cells with UV to induce p38α pathway activation and MK2 degradation. We found that only cells deficient for MDM2, but not the other two E3 ligases, showed enhanced MK2 protein levels after UV irradiation (Fig. 6A). Accordingly, knockdown of this E3 ligase partially recovered the levels of MK2 in p38α KO cells (Fig. 6B), pointing to MDM2 as a potential regulator of the degradation of MK2 when separated from p38α.

Next, we used purified recombinant proteins to confirm that MK2 was a direct substrate of MDM2. We found that MK2 was ubiquitinated by MDM2 in vitro to a similar extent to p53, a well-known MDM2 substrate (45, 46) (Fig. 6C and Fig. S4C). Moreover, using mass spectrometry analysis, we found that K188, K371, K374 and K385 were ubiquitinated upon incubation with MDM2 (Fig. 6D and Fig. S5). Interestingly, structural analysis indicated that these four lysines are buried inside the p38α-MK2 complex. Specifically, K188 is buried within the dimerization interface, while K371, K374 and K385 are located in the MK2 D-motif that also interacts with p38α (Fig. 6E). Therefore, these sites will be difficult to ubiquitinate when MK2 is bound to p38α, explaining why MK2 can only be targeted (and degraded) by MDM2 once it is released from p38α. To confirm that MDM2 can ubiquitinate these residues, we generated a MK2 mutant with the four lysines mutated to arginines (MK2 4K/R), and found that MK2 ubiquitination was significantly impaired in the 4K/R mutant compared to the WT protein (Fig. 6F), indicating that the identified lysines are involved in MK2 ubiquitination by MDM2.

Irreversible degradation of MK2 facilitates cell death upon severe stress. Our results demonstrate that MK2 regulation is mainly dictated by protein stability, which in turn depends on its interaction with p38α to form a stable complex that avoids its ubiquitination by MDM2. Moreover, we have shown that sustained p38α activation and the consequent irreversible loss of MK2 correlates with cell death. Therefore, we hypothesized that MK2 activity has a protective role in stress, and its degradation-mediated inactivation would impair cell survival. To test this idea, we used the MK2 4K/R mutant that exhibits a defective ubiquitination pattern and it is predicted to show increased protein stability upon dissociation from p38α. MK2 KO MEFs were reconstituted with MK2 WT or the 4K/R mutant and then were irradiated with a high UV dose to induce sustained p38α pathway activation, which results in complex dissociation and cell death.

We observed that the levels of the MK2 4K/R mutant were not substantially reduced following UV irradiation, at least during the time analyzed, confirming that this mutant was more stable than its WT counterpart (Fig. 7A). Interestingly, cells expressing this more stable 4K/R form showed reduced UV-induced cell death compared to cells expressing MK2 WT (Fig. 7B). These results support the hypothesis that stabilization of MK2, and therefore a higher and/or more sustained MK2 activity, results in enhanced cell viability in response to stress.

To confirm this idea, cells were stimulated with high doses of UV in the presence of p38α or MK2 inhibitors. In agreement with MK2 having a pro-survival role, blocking the activity of either p38α or MK2 increased the UV-induced cell death (Fig. 7C). Of note, p38α inhibition avoids MK2 phosphorylation and therefore MK2 protein levels were increased in these cells (Fig. 7D). However, the MK2 that accumulates is not phosphorylated, lacks kinase activity, and therefore cannot exert its pro-survival function, explaining the increased cell death observed despite MK2 protein accumulation. Altogether, our results indicate that MK2 signaling regulates the viability of stressed cells. Since sustained stress is deleterious for cells, it is conceivable that MK2 degradation serves as regulatory mechanism to limit this pro-survival function, eventually leading to cell death of the irreversibly damaged cells.

DISCUSSION

Consistent with the evidence implicating p38α and MK2 in the regulation of many cellular stress responses, aberrant activation of this pathway has been connected to several human diseases such as inflammatory disorders and cancer (24, 25, 47). It is therefore important for cellular and organismal homeostasis that the activity of the p38α-MK2 pathway is strictly controlled. It is known that p38α can be inactivated by several types of phosphatases, whose expression sometimes can be induced by p38α signaling itself (21, 22), and negative feedback loops can further modulate the pathway activity (18, 20). In contrast, very little is known on how MK2 activity is physiologically shut-off. Of note, MK2 amplification correlates with poor prognosis in some tumors, and high MK2 levels in multiple myeloma are required for tumor growth and drug resistance (48, 49). Hence, dysregulated MK2 expression can alter cell homeostasis leading to disease, supporting the importance of elucidating the mechanisms that control MK2 activity to understand the implication of the p38α-MK2 pathway in pathogenesis.

Our results show a key role for proteolysis in controlling the extent of MK2 activity. In homeostasis, endogenous MK2 and p38α form a complex. When the pathway is activated, p38α phosphorylates MK2 leading to complex dissociation and the two kinases become available to phosphorylate their respective downstream targets. We demonstrate that upon separation from p38α, MK2 can be ubiquitinated, which triggers its degradation by the proteasome. A decreased number of phosphorylated (active) MK2 molecules in the cell ensures that the signal is turned off. Interestingly, the inactivation of p38α and MK2 seems to be based on different mechanisms offering the opportunity to specifically target MK2-regulated functions such as cytokine production or RNA metabolism, without affecting functions regulated by other p38α substrates. Our study has focused on MK2, one of the best characterized effectors of p38α, but a similar mechanism could operate for other substrates that can associate with p38α in a stable manner, as it might be the case for MK3, which contains a similar docking motif to MK2 (50). However, other proteins that interact with p38α seem to be regulated in completely different ways, as shown for MKK6 (18) and ATF2 (51), despite also having a docking motif. It should be noted that the ability of endogenous MK2 to form a stable complex with p38α in non-stimulated cells has not been reported for other substrates.

We identify the E3 ubiquitin ligase MDM2 as an important regulator of MK2 protein stability. We found that MDM2 can ubiquitinate MK2 on four lysine residues that are predicted to be buried inside the interface between MK2 and p38α, which is consistent with the fact that MK2 is only degraded when separated from p38α. MDM2 is a critical regulator of the p53 protein in response to various stress signals (52, 53). Given that the p53 and p38α-MK2 pathways have a key role in safeguarding cellular homeostasis, MDM2 stands as a common regulator to engage an integrated cellular response to stress. Accordingly, it is tempting to propose that MDM2 could function as a hub that coordinates the pro-survival role of MK2 signaling with the apoptotic programs driven by p53.

Our work indicates that the dynamic interaction between p38α and MK2 is regulated by the kinetics of p38α activation (transient versus sustained) and makes an important contribution to the pathway output (Fig. S6). Thus, MK2 levels are recovered when the pathway is transiently activated, such as in response to cytokine stimulation (54). In this scenario, the MK2 mRNA accumulates, probably due to transcriptional activation, allowing the re-expression of MK2

protein when p38α is no longer active. Newly synthesized MK2 then binds to de-phosphorylated p38α forming a heterodimer again and restoring cell homeostasis. However, under conditions of persistent or severe stress (55, 56), p38α activation is sustained and MK2 cannot bind to the phosphorylated p38α leading to irreversible MK2 downregulation and cell death. Importantly, it has been recently reported that mice expressing a constitutively active p38α mutant show reduced MK2 expression levels in several tissues, which correlates with a significant body weight loss, suggesting that the mechanism of MK2 downregulation that we propose may also operate in vivo (57). Of note, in response to sustained stress, MDM2 has been reported to show decreased affinity for phosphorylated p53 (58), suggesting that it could shut-down the MK2 pro-survival role without affecting the p53-regulated pro-apoptotic program.

The ability to facilitate the survival of cells subjected to stress is a conserved function of the p38α pathway. In response to genotoxic stress such as UV, MK2 has been reported to activate the G_2/M cell cycle checkpoint via Cdc25B/C phosphorylation (3), and can also phosphorylate the RNA-binding proteins NELFE and RBM7, enabling a RNA polymerase II transcriptional response that is crucial for the survival of stressed cells (4, 59). Furthermore, phosphorylation of the tumor necrosis factor receptor-interacting kinase RIPK1 by MK2 suppresses the pro-apoptotic and pro-necroptotic functions of this key molecule upon inflammatory and stress stimuli (27). These mechanisms could potentially explain the pro-survival role of the p38α-MK2 pathway that we observe following severe stress. However, in some cell types, p38α signaling has been reported to contribute to UV-induced apoptosis, which has been related to p53 (60, 61) or to changes in pro-apoptotic molecules and survival signals (62). Therefore, it is conceivable that the cell type, the duration of the stimulus, and the interplay with other signaling pathways may all contribute to define the final outcome of p38α activation in stressed cells. In line with this idea, there is evidence that in vivo roles of MK2 are highly dependent on the context. For example, lack of MK2 can protect mouse skin from UV-B-induced keratinocyte death (6), but enhances DNA damage and chemotherapy cytotoxicity in KRAS-induced lung tumors (63). In fact, the function of MK2 has been reported to depend on the genetic background, and in particular p53 status (64).

It is important to note that p38α is not the only signaling pathway that controls DNA damage-induced cell death. For example, cell-to-cell variability in JNK activity has been proposed to contribute to the timing and probability of death in UV-exposed cells (65). Our

results suggest that the MK2 protein expression levels, as determined by the extent of p38α activation, may provide an additional source of variability that affects the biological outcome. However, considering that MK2 in several cell types can potentially contribute to resolving tissue damage (66), it is difficult to predict the consequences of interfering with MK2 activity in vivo.

In summary, we describe a new layer of regulation of the p38α signaling pathway, which is based on the balance between MK2 protein degradation and de novo synthesis, and controls its ability to modulate the cellular response to stress. This mechanism relies on the ability of p38α to bind to and stabilize MK2, which is required to recover cell homeostasis. The inability to re-assemble the p38-MK2 complex in response to strong or sustained stress, may function as a sensor of irreversible damage leading to cell death.

METHODS

Cell treatments. To deplete p38α, *Mapk14*$^{lox/lox}$ UBC-Cre-ERT2 CAFs were treated with 100 nM 4-hydroxytamoxifen (Sigma, # H7904-5MG) for 48 h. For the inhibition of p38α, we used 2 μM PH797804 (Selleckchem, #S2726), 10 μM SB203580 (Axon MEDCHEM, #1363) or 10 μM BIRB796 (Axon MedChem #1358). MK2 was inhibited using 2.5 μM PF3644022 (Sigma, #PZ0188) or 10 μM MK2 III (Calbiochem). The activation of the p38α pathway was induced by exposure to UV either 10 J/m^2 or 30 J/m^2, using a UVC-500 crosslinker (Amersham Biosciences), 200 mM NaCl, 100 μM Hydrogen peroxide (Sigma #H1009), 20 μM anisomycin (Sigma, #A9789), 10 ng/ml LPS (Sigma #L4005) or 5 ng/ml TGF-β1 (Prepotech, #100-21). The proteasome was inhibited with 20 μM MG132 (Sigma #C2211), 100 nM Bortezamib (Selleckchem, #PS-341), 3 μM b-AP15 (Selleckchem, # S4920) or 200 μM O-phenanthroline (MERK Millipore, #516705). To inhibit autophagy, we used 400 nM Bafilomycin A1 (Sigma, #B1793).

MK2 immunoprecipitation. To immunoprecipitate endogenous MK2, we used single-domain antibodies against MK2 bound to agarose beads (MK2-trap_A, Chromotek, #mta-20). As a control, we used the same agarose beads (Chromotek, #bab-20). Cells or tissue samples were lysed and processed as recommended in the manufacturer's protocol. Briefly, cell lysates were extracted with the buffer provided, and protein content was quantified using the RC DC Protein

Assay Kit I (Bio-Rad #5000111)**.** 25 µl of MK2-Trap_A or control agarose beads were incubated overnight with 500 µg of cell lysate rotating at 4ºC. The next day, beads were recovered, washed three times, resuspended in 1x SDS-PAGE sample buffer and heated for 5 min at 95°C. Immunoprecipitated proteins were analyzed by immunoblotting.

Sucrose gradients. CAFs were trypsinized, harvested and resuspended in 25 mM HEPES, 0.1 mM EDTA, 12.5 mM $MgCl_2$, 10% Glycerol, 0.1 M KCl, 0.1% NP-40, 1 mM DTT and 1x EDTA-free complete protease inhibitor cocktail (Roche, #1187358000). Lysates were incubated for 15 min on ice and centrifuged 15 min at 16000 xg. The supernatant (1 mg) was loaded on top of a 4 ml linear sucrose gradient (20–28%) in the same buffer. Gradients were centrifuged at 156,500 xg in a Beckman Coulter MLS-50 rotor for 16 h at 4 °C. Fractions of 930 µl were collected from top to bottom and were analyzed by immunoblotting.

Determination of the MK2 protein half-life. CAFs were treated or not with p38α inhibitor and exposed to CHX (50 µM, Sigma, #C6255). Cells were collected at different times and subjected to immunoblotting with an MK2 antibody, using Tubulin as a loading control. The intensity of the bands was determined using the ImageJ software. The half-life was determined by fitting the data to an exponential decay equation using the GraphPad Prism computer program (Graphpad Software, Inc., La Jolla, CA, USA).

Downregulation of E3 ubiquitin ligases by siRNAs. U2OS cells or p38α KO CAFs were transfected with siRNAs using Lipofectamine RNAi MAX transfection reagent (ThermoFisher, #13778150) following the manufacturer's protocol. After transfection, cells were incubated 24 h in antibiotic free media, split and analyzed 48 h later. The following siRNAs were purchased from Ambion Life Technologies: SMURF1 5'ccagcacuaugaucuauautt 3' (#120615); STUB1 5' gagcuaugaugaggccauctt 3' (#215047); MDM2 5'gccauugcuuuugaaguuatt 3'(#122296).

In vitro Ubiquitin conjugation reaction. Ubiquitination reactions were performed by using an MDM2/p53 Ubiquitination kit following the manufacturer's protocol (Boston Biochem, #K-200B). Briefly, recombinant E1, E2 and GST-MDM2 were incubated with either His-p53, GST-

MK2 or GST-MK2 4K/R for 60 min at 37ºC. The reaction was terminated by adding 1x SDS-PAGE sample buffer and heating at 95ºC for 5 min. Samples were analyzed in a 10% polyacrylamide gel that was run for 5 h, followed by immunoblotting with antibodies against p53 or MK2. GST-MK2 and GST-MK2 4K/R were expressed in *E.coli* and purified following standard protocols.

CellTrace CFSE-based proliferation assays. Carboxyfluorescein succinimidyl ester (CFSE) was used to measure cell proliferation. Each time that a cell divides, CFSE is transferred equally among the daughter cells, reducing fluorescence in half. Typically, up to 10^6 cells/ml were labeled with 1 μl of CFSE (Thermofisher #C34554) and incubated for 24 h. The next day, control cells were collected and analyzed by flow cytometry while the rest of the cells were treated with either low UV or high UV doses and incubated for 24, 48, 72 and 96 h. After the incubation time, cells were analyzed by flow cytometry using exactly the same protocol as for control cells.

Cell viability assays. U2OS cells were trypsinized and $3x10^5$ cells were plated in triplicate in 6 well plates. Cells were incubated for 24 h and then were irradiated with the indicated doses of UV, and allowed to grow for 7 days. Then cells were fixed in 4% paraformaldehyde (Aname, 15710) and stained with crystal Violet (Sigma, HT90132). The colony area was measured using ImageJ.

Statistical analysis. Data are expressed as average ± SEM. Statistical analysis was performed by using a two-tailed Student's t-test (Mann-Whitney) for the comparison of two groups or ANOVA using Bonferroni post-hoc correction for multiple groups using GraphPad Prism Software 6.01 (GraphPad Software, Inc., La Jolla CA). p-values are expressed as *, $p \leq 0.05$, **, $p \leq 0.01$, and ***, $p \leq 0.001$.

Data Availability. All relevant data, associated protocols, and materials are within the manuscript and its SI Appendix.

ACKNOWLEDGEMENTS

We thank Bernat Crosas (IBMB-CSIC) for insightful suggestions on ubiquitination assays, Sergi Regot (Johns Hopkins University School of Medicine) for the p38α-KTR reporter, Jessica Vitos-Faleato and Nevenka Radic for critical reading of the manuscript and helpful discussions, Raquel Batlle for the generation of MSCs and all members of the Nebreda laboratory for support and discussions. We are grateful to Marina Gay, Marta Vilaseca and members of the IRB Mass spectrometry and proteomics facility for the identification of MK2 ubiquitinated residues. We acknowledge the excellent technical assistance of the UB Fluorescence-Activated Cell Sorting Flow cytometry facility. This work was supported by grants from the European Research Council (294665), the Spanish Ministerio de Ciencia e Innovación (MICINN, SAF2016-81043-R and PID2019-109521RB-I00), and AGAUR (2017 SRG-557). IRB Barcelona is the recipient of institutional funding from MINECO through the Centres of Excellence Severo Ochoa award and from the CERCA Program of the Catalan Government.

AUTHOR CONTRIBUTIONS

N.G.-P. designed and performed most of the experiments, analyzed data and wrote the manuscript. M.C.-R. performed key experiments, analyzed data, provided critical feedback, and contributed to writing the manuscript. B.C performed key experiments, analyzed data, generated CAFs and BBL358 cells, provided critical feedback, and contributed to writing the manuscript. A.K. performed molecular simulations. J.G. generated p38α mutants. A.I. provided CAFs. E.L. provided technical support. M.G. provided essential reagents and advice. A.R.N. provided funding, supervised the overall study, designed experiments, analyzed data, and wrote the manuscript.

The authors declare no conflict of interests.

REFERENCES

1. N. Trempolec, N. Dave-Coll, A. R. Nebreda, SnapShot: p38 MAPK Substrates. *Cell* **152**, 924-924.e921 (2013).
2. J. Han, J. Wu, J. Silke, An overview of mammalian p38 mitogen-activated protein kinases, central regulators of cell stress and receptor signaling. *F1000Res* **9**, F1000 Faculty Rev-1653 (2020).

3. I. A. Manke *et al.*, MAPKAP kinase-2 is a cell cycle checkpoint kinase that regulates the G2/M transition and S phase progression in response to UV irradiation. *Mol Cell* **17**, 37-48 (2005).
4. M. E. Borisova *et al.*, p38-MK2 signaling axis regulates RNA metabolism after UV-light-induced DNA damage. *Nat Commun* **9**, 1017 (2018).
5. N. Trempolec *et al.*, Induction of oxidative metabolism by the p38α/MK2 pathway. *Sci Rep* **7**, 11367 (2017).
6. F. Köpper *et al.*, Damage-induced DNA replication stalling relies on MAPK-activated protein kinase 2 activity. *Proc Natl Acad Sci USA* **110**, 16856 (2013).
7. E. Rodríguez-Carballo, B. Gámez, F. Ventura, p38 MAPK Signaling in Osteoblast Differentiation. *Front Cell Dev Biol* **4**, 40-40 (2016).
8. F. B. Engel *et al.*, p38 MAP kinase inhibition enables proliferation of adult mammalian cardiomyocytes. *Genes Dev* **19**, 1175-1187 (2005).
9. B. Canovas, A. R. Nebreda, Diversity and versatility of p38 kinase signalling in health and disease. *Nat Rev Mol Cell Biol* 10.1038/s41580-020-00322-w, 1-21, doi: 10.1038/s41580-41020-00322-w (2021).
10. Jeremy E. Purvis, G. Lahav, Encoding and Decoding Cellular Information through Signaling Dynamics. *Cell* **152**, 945-956 (2013).
11. J. R. Perkins, I. Diboun, B. H. Dessailly, J. G. Lees, C. Orengo, Transient Protein-Protein Interactions: Structural, Functional, and Network Properties. *Structure* **18**, 1233-1243 (2010).
12. J. Westermarck, J. Ivaska, G. L. Corthals, Identification of protein interactions involved in cellular signaling. *Mol Cell Proteomics* **12**, 1752-1763 (2013).
13. K. Stojanovski *et al.*, Interaction Dynamics Determine Signaling and Output Pathway Responses. *Cell Rep* **19**, 136-149 (2017).
14. A. White, C. A. Pargellis, J. M. Studts, B. G. Werneburg, B. T. Farmer, Molecular basis of MAPK-activated protein kinase 2:p38 assembly. *Proc Natl Acad Sci USA* **104**, 6353-6358 (2007).
15. G. Tan, J. Niu, Y. Shi, H. Ouyang, Z. H. Wu, NF-kappaB-dependent microRNA-125b up-regulation promotes cell survival by targeting p38alpha upon ultraviolet radiation. *J Biol Chem* **287**, 33036-33047 (2012).
16. A. Kuzmanic *et al.*, Changes in the free-energy landscape of p38α MAP kinase through its canonical activation and binding events as studied by enhanced molecular dynamics simulations. *eLife* **6**, e22175 (2017).
17. P. Sok *et al.*, MAP Kinase-Mediated Activation of RSK1 and MK2 Substrate Kinases. *Structure* **28**, 1101-1113 (2020).
18. C. Ambrosino *et al.*, Negative feedback regulation of MKK6 mRNA stability by p38alpha mitogen-activated protein kinase. *Mol Cell Biol* **23**, 370-381 (2003).
19. J. H. Hu *et al.*, Feedback control of MKP-1 expression by p38. *Cell Signal* **19**, 393-400 (2007).
20. P. C. Cheung, D. G. Campbell, A. R. Nebreda, P. Cohen, Feedback control of the protein kinase TAK1 by SAPK2a/p38alpha. *EMBO J* **22**, 5793-5805 (2003).
21. C. J. Caunt, S. M. Keyse, Dual-specificity MAP kinase phosphatases (MKPs): shaping the outcome of MAP kinase signalling. *FEBS J* **280**, 489-504 (2013).
22. A. Cuadrado, A. R. Nebreda, Mechanisms and functions of p38 MAPK signalling. *Biochem J* **429**, 403-417 (2010).

23. W. Fan *et al.*, Hsp70 Interacts with Mitogen-Activated Protein Kinase (MAPK)-Activated Protein Kinase 2 To Regulate p38MAPK Stability and Myoblast Differentiation during Skeletal Muscle Regeneration. *Mol Cell Biol* **38**, pii: e00211-00218. (2018).
24. A. Cuenda, S. Rousseau, p38 MAP-kinases pathway regulation, function and role in human diseases. *Biochim Biophys Acta* **1773**, 1358-1375 (2007).
25. J. Gupta, A. R. Nebreda, Roles of p38alpha mitogen-activated protein kinase in mouse models of inflammatory diseases and cancer. *FEBS J* **282**, 1841-1857 (2015).
26. P. Trulley *et al.*, Alternative Translation Initiation Generates a Functionally Distinct Isoform of the Stress-Activated Protein Kinase MK2. *Cell Rep* **27**, 2859-2870 e2856 (2019).
27. M. B. Menon, M. Gaestel, MK2–TNF–Signaling Comes Full Circle. *Trends Biochem Sci* **43**, 170-179 (2018).
28. K. Soukup *et al.*, Loss of MAPK-activated protein kinase 2 enables potent dendritic cell-driven anti-tumour T cell response. *Sci Rep* **7**, 11746 (2017).
29. L. Latonen, Y. Taya, M. Laiho, UV-radiation induces dose-dependent regulation of p53 response and modulates p53-HDM2 interaction in human fibroblasts. *Oncogene* **20**, 6784-6793 (2001).
30. S. Regot, Jacob J. Hughey, Bryce T. Bajar, S. Carrasco, Markus W. Covert, High-Sensitivity Measurements of Multiple Kinase Activities in Live Single Cells. *Cell* **157**, 1724-1734 (2014).
31. S. M. Lukas *et al.*, Catalysis and function of the p38 alpha.MK2a signaling complex. *Biochemistry* **43**, 9950-9960 (2004).
32. S. Lopez-Aviles *et al.*, Activation of Srk1 by the mitogen-activated protein kinase Sty1/Spc1 precedes its dissociation from the kinase and signals its degradation. *Mol Biol Cell* **19**, 1670-1679 (2008).
33. T. Moriguchi *et al.*, Purification and identification of a major activator for p38 from osmotically shocked cells. *J. Biol Chem.* **271**, 26981-26988 (1996).
34. T. Sudo, K. Kawai, H. Matsuzaki, H. Osada, p38 mitogen-activated protein kinase plays a key role in regulating MAPKAPK2 expression. *Biochem Biophys Res Commun* **337**, 415-421 (2005).
35. P. R. Mittelstadt, H. Yamaguchi, E. Appella, J. D. Ashwell, T cell receptor-mediated activation of p38{alpha} by mono-phosphorylation of the activation loop results in altered substrate specificity. *J. Biol Chem* **284**, 15469-15474 (2009).
36. I. Dikic, Proteasomal and Autophagic Degradation Systems. *Annu Rev Biochem* **86**, 193-224 (2017).
37. I. Livneh, V. Cohen-Kaplan, C. Cohen-Rosenzweig, N. Avni, A. Ciechanover, The life cycle of the 26S proteasome: from birth, through regulation and function, and onto its death. *Cell Res* **26**, 869-885 (2016).
38. G. Ben-Nissan, M. Sharon, Regulating the 20S Proteasome Ubiquitin-Independent Degradation Pathway. *Biomolecules* **4**, 862-884 (2014).
39. A. M. Pickering, K. J. Davies, Degradation of damaged proteins: the main function of the 20S proteasome. *Prog Mol Biol Transl Sci* **109**, 227-248 (2012).
40. X. Wang *et al.*, The 19S Deubiquitinase inhibitor b-AP15 is enriched in cells and elicits rapid commitment to cell death. *Mol Pharmacol* **85**, 932-945 (2014).
41. Y. Song *et al.*, Blockade of deubiquitylating enzyme Rpn11 triggers apoptosis in multiple myeloma cells and overcomes bortezomib resistance. *Oncogene* **36**, 5631-5638 (2017).

42. K. I. Nakayama, K. Nakayama, Ubiquitin ligases: cell-cycle control and cancer. *Nat Rev Cancer* **6**, 369-381 (2006).
43. C. E. Berndsen, C. Wolberger, New insights into ubiquitin E3 ligase mechanism. *Nat Struct Mol Biol* **21**, 301-307 (2014).
44. Y. Li *et al.*, An integrated bioinformatics platform for investigating the human E3 ubiquitin ligase-substrate interaction network. *Nat Commun* **8**, 347 (2017).
45. Y. Haupt, R. Maya, A. Kazaz, M. Oren, Mdm2 promotes the rapid degradation of p53. *Nature* **387**, 296-299 (1997).
46. M. H. Kubbutat, S. N. Jones, K. H. Vousden, Regulation of p53 stability by Mdm2. *Nature* **387**, 299-303 (1997).
47. M. Gaestel, What goes up must come down: molecular basis of MAPKAP kinase 2/3-dependent regulation of the inflammatory response and its inhibition. *Biol Chem* **394**, 1301-1315 (2013).
48. B. Liu *et al.*, A Functional Copy-Number Variation in MAPKAPK2 Predicts Risk and Prognosis of Lung Cancer. *Am J Hum Genet* **91**, 384-390 (2012).
49. M. Guo *et al.*, Targeting MK2 Is a Novel Approach to Interfere in Multiple Myeloma. *Front Oncol* **9**, 722 (2019).
50. N. Ronkina *et al.*, The mitogen-activated protein kinase (MAPK)-activated protein kinases MK2 and MK3 cooperate in stimulation of tumor necrosis factor biosynthesis and stabilization of p38 MAPK. *Mol Cell Biol* **27**, 170-181 (2007).
51. K. Kirsch *et al.*, Co-regulation of the transcription controlling ATF2 phosphoswitch by JNK and p38. *Nat Commun* **11**, 5769 (2020).
52. M. F. Lavin, N. Gueven, The complexity of p53 stabilization and activation. *Cell Death Differ* **13**, 941-950 (2006).
53. H. F. Horn, K. H. Vousden, Coping with stress: multiple ways to activate p53. *Oncogene* **26**, 1306-1316 (2007).
54. T. Tomida, M. Takekawa, H. Saito, Oscillation of p38 activity controls efficient pro-inflammatory gene expression. *Nat Commun* **6**, 8350 (2015).
55. H. Ju *et al.*, Sustained activation of p38 mitogen-activated protein kinase contributes to the vascular response to injury. *J Pharmacol Exp Ther* **301**, 15-20 (2002).
56. M. Warny *et al.*, p38 MAP kinase activation by Clostridium difficile toxin A mediates monocyte necrosis, IL-8 production, and enteritis. *J Clin Invest* **105**, 1147-1156 (2000).
57. I. Darlyuk-Saadon *et al.*, Expression of a constitutively active p38alpha mutant in mice causes early death, anemia, and accumulation of immunosuppressive cells. *FEBS J* 10.1111/febs.15697, doi: 10.1111/febs.15697 (2021).
58. U. M. Moll, O. Petrenko, The MDM2-p53 Interaction. *Mol Cancer Res* **1**, 1001-1008 (2003).
59. A. Bugai *et al.*, P-TEFb Activation by RBM7 Shapes a Pro-survival Transcriptional Response to Genotoxic Stress. *Mol Cell* **74**, 254-267 e210 (2019).
60. D. V. Bulavin *et al.*, Phosphorylation of human p53 by p38 kinase coordinates N-terminal phosphorylation and apoptosis in response to UV radiation. *EMBO J* **18**, 6845-6854 (1999).
61. X. Gong, X. Ming, P. Deng, Y. Jiang, Mechanisms regulating the nuclear translocation of p38 MAP kinase. *J Cell Biochem* **110**, 1420-1429 (2010).
62. A. Porras *et al.*, P38 alpha mitogen-activated protein kinase sensitizes cells to apoptosis induced by different stimuli. *Mol Biol Cell* **15**, 922-933 (2004).

63. Y. W. Kong *et al.*, Enhancing chemotherapy response through augmented synthetic lethality by co-targeting nucleotide excision repair and cell-cycle checkpoints. *Nat Commun* **11**, 4124 (2020).
64. H. C. Reinhardt, A. S. Aslanian, J. A. Lees, M. B. Yaffe, p53-Deficient Cells Rely on ATM- and ATR-Mediated Checkpoint Signaling through the p38MAPK/MK2 Pathway for Survival after DNA Damage. *Cancer Cell* **11**, 175-189 (2007).
65. H. Miura, Y. Kondo, M. Matsuda, K. Aoki, Cell-to-Cell Heterogeneity in p38-Mediated Cross-Inhibition of JNK Causes Stochastic Cell Death. *Cell Rep* **24**, 2658-2668 (2018).
66. T. Thuraisingam *et al.*, MAPKAPK-2 signaling is critical for cutaneous wound healing. *J Invest Dermatol* **130**, 278-286 (2010).

Figure legends

Fig. 1. Sustained p38α activation leads to irreversible MK2 downregulation. **(A-B)** Cancer-associated fibroblasts (CAFs) were stimulated with UV-C (30 J/m^2) (**A**) or anisomycin (20 μM) (**B**) for the indicated times, and cell lysates were analyzed by immunoblotting. The images shown are representative of two independent experiments. The upper band recognized by phospho-p38 antibodies was not consistently detected. **(C**) CAFs, U2OS and BBL358 cells were treated with UV-C (30 J/m^2), anisomycin (20 μM), H_2O_2 (100 μM) or NaCl (200 mM) for 4 h, or were left untreated (NT). Cell lysates were analyzed by immunoblotting. The images shown are representative of two independent experiments. **(D)** Four mammary tumors (1-4) were obtained from two different mice expressing MMTV-PyMT and were immediately treated with 300 mM NaCl for 15 min or left untreated (NT), homogenized and analyzed by immunoblotting. Band intensities were analyzed by ImageJ and the MK2/Tubulin ratios were represented in the histograms. When two MK2 bands were detected, the lower one (shorter isoform) was considered for quantification. The asterisk indicates a non-specific band.

Fig. 2. Transient p38α activation allows MK2 expression recovery. **(A)** Bone-marrow derived macrophages (BMDMs) were starved for 17 h, and then stimulated with Lipopolysaccharide (LPS, 10 ng/ml) for the indicated times. Cell lysates were analyzed by immunoblotting. Band intensities were analyzed by ImageJ and the MK2/Tubulin ratios were represented in the histogram. The images shown are representative of two independent experiments. **(B)** BMDMs were isolated from 5 different mice and treated as in (**A**). RNA was extracted and the MK2 mRNA levels were determined by qRT-PCR. Data is shown as mean ± SEM. **(C)** Cancer-associated fibroblasts (CAFs) were starved overnight in medium containing 0.5% fetal bovine serum and then treated with Transforming growth factor (TGF)-β (5 ng/μl) for the indicated times. Cell lysates were analyzed by immunoblotting. Phospho-Smad 3 antibody was used to confirm TGFβ pathway activation. The histogram represents the MK2/Tubulin ratio determined as in (**A**). The images shown are representative of two independent experiments. **(D)** CAFs were treated with TGFβ as in (**C**) and MK2 mRNA levels were determined by qRT-PCR. Data is shown as mean ± SEM of five independent experiments. The lower MK2 band (shorter isoform) was considered for quantification.

Fig. 3. The extent of p38α activation shapes MK2 levels and cell fate following stress. **(A)** U2OS cells were exposed to UV-C, 10 J/m^2 (UV10) or 30 J/m^2 (UV30) doses, and then were incubated for the indicated times. Cell lysates were analyzed by immunoblotting. Band intensities were analyzed by ImageJ and the MK2/Tubulin ratios were represented in the histograms. The images shown are representative of two independent experiments. **(B)** U2OS cells were stained with the CellTrace CFSE dye and incubated for 24 h. Then, cells were either directly analyzed for CFSE incorporation (0 h) or exposed to UV10 or UV30 as in (**A**), and analyzed 24, 48, 72 and 96 h later. The intensity of CFSE florescence decreases as peaks move to the left, indicating cell proliferation, and the pick area correlates with the number of cells analyzed. Different times are shown by different colors. The histograms shown are representative data of two independent experiments. **(C)** U2OS cells were exposed to UV10 or UV30 or left untreated (NT), and then were plated to form colonies, which were analyzed 7 days later. The graph shows the colony area relative to NT cells. Data represents mean ± SEM of three independent experiments. **(D)** U2OS cells were transfected with a p38α activity reporter (30) and then were exposed to UV10 or UV30. Single cells were analyzed by time-lapse microscopy for the indicated times. Black ends represent cells that die. The p38α activity status is shown in red (active) or blue (inactive). **(E)** U2OS cells were treated with UV10 or UV30, and 24 h later were collected for DAPI staining followed by FACs analysis. The percentages of dead and alive cells are indicated. Representative images of dead (DAPI$^+$) and alive (DAPI$^-$) cells are shown (upper image). **(F)** U2OS cells were treated with UV10 or UV30 and 24 h later floating and poorly-attached cells (dead) were separated from the well-attached cells (alive). Lysates from the two cell populations and were analyzed by immunoblotting. The histogram represents MK2/Tubulin ratios determined as in (**A**). The images shown are representative of three independent experiments

Fig. 4. MK2 levels are regulated by its interaction with p38α. (**A**-**B**) Lysates from cancer-associated fibroblasts (CAFs) **(A)** and the indicated mouse tissues (**B**) were immunoprecipitated with MK2-Trap_A (MK2) or agarose beads (Beads), and then were analyzed by immunoblotting. **(C)** CAFs were treated with UV-C 30 J/m^2 (UV30) and the cell lysates were immunoprecipitated with MK2-Trap_A (IP MK2), and then analyzed by immunoblotting. Band intensities were analyzed by ImageJ and the p38α/MK2 ratios are indicated. **(D)** CAFs were treated with UV30

for the indicated times and lysates were separated on 20-28% sucrose gradients. Collected fractions were analyzed by immunoblotting. PSMD11 was used as a marker for high molecular weight complexes. Band intensities were analyzed by ImageJ. The histograms show the p38α and MK2 levels in fractions 1 and 2, which are normalized to the total p38α and MK2 amounts in untreated cells (NT). Data represents mean ± SEM of two independent experiments. **(E)** CAFs were pre-treated with the p38 inhibitor BIRB796 (p38 inh, 10 μM) to preserve the p38α-MK2 complex, or the vehicle DMSO for 2 h and then incubated with cycloheximide (CHX, 50 μg/ml), which induces p38α activation and complex separation. At the indicated times, lysates were analyzed by immunoblotting. The estimated MK2 half-lifes are indicated (t 1/2). Data represents mean ± SEM of three independent experiments. **(F)** Lysates from WT and p38α KO CAFs were separated on 20-28% sucrose gradients. Collected fractions were analyzed by immunoblotting. The asterisk in the blot indicates a non-specific band. The 26S proteasome component PSMD11 was used as a marker for high molecular weight complexes. Band intensities were analyzed by ImageJ software. The histogram shows the quantifications of the MK2 levels in fractions 1 and 2, which are normalized to the total MK2 amount in WT cells. Data represents mean ± SEM of three independent experiments. Significant differences refer to fraction 2. **(G)** WT and p38α KO CAFs expressing Myc-p38α WT or the mutants K53M (KM) and Thr180A/Y182F (TY), or a GFP-expressing vector as control, were either left untreated or treated with UV30 for 1 h. Cell lysates were analyzed by immunoblotting. Band intensities were analyzed by ImageJ and the MK2/Tubulin ratios are represented in the histogram. Data represents mean ± SEM of three independent experiments. When two MK2 bands were detected, the lower one (shorter isoform) was considered for quantification.

Fig. 5. MK2 is degraded by the proteasome upon dissociation from p38α. **(A)** WT cancer-associated fibroblasts (CAFs) were treated with the proteasome inhibitor Bortezomib, (BTZ, 100 nM) or the autophagy inhibitor Bafilomycin A1 (BAF, 400 nM), stimulated with UV-C 30 J/m^2 (UV30), and then incubated for the indicated times. Lysates were analyzed by immunoblotting. Ubiquitinated (Ub) and LC3II proteins were used as markers for proteasome or autophagy inhibition, respectively. The arrowhead indicates LC3II accumulation. The upper band recognized by phospho-p38 antibodies was not consistently detected. **(B)** CAFs were pre-treated with BTZ for 2 h, irradiated with UV30 and then incubated for 4 h. Cell lysates were

immunoprecipitated with MK2-Trap_A (MK2) or agarose beads (Beads), and analyzed by immunoblotting. **(C)** WT and p38α KO CAFs were treated with the proteasome inhibitor MG132 (MG, 20 μM) and BAF for 16 h, and lysates were analyzed by immunoblotting. p53 and LC3II proteins were used as markers for proteasome and autophagy inhibition, respectively. **(D)** U2OS cells were pre-treated with MG and then stimulated with UV30 for 2 and 4 h. Cell lysates were analyzed by immunoblotting. **(E)** CAFs were pre-incubated with the proteasome inhibitors MG, BTZ, b-AP15 (AP, 3 μM) or O-phenanthroline (OPA, 200 μM) for 2 h, irradiated with UV30 and then incubated for 4 h. Cell lysates were analyzed by immunoblotting. Ubiquitinated (Ub) proteins were used as a control for proteasome inhibition. **(F)** CAFs were pre-incubated with the proteasome inhibitors MG, BTZ, AP or OPA for 6 h. Cell lysates were analyzed by immunoblotting with p53 antibodies to confirm proteasome inhibition. In all cases, the images shown are representative from two independent experiments, band intensities were analyzed by ImageJ and the lower MK2 band (shorter isoform) was considered for quantification.

Fig. 6. MDM2 ubiquitinates MK2. **(A)** U2OS cells were transfected with siRNAs against MDM2, SMURF1 and STUB1, or a non-targeting control, stimulated with UV-C, 30 J/m^2 (UV30) and then incubated for 4 h. Cell lysates were analyzed by immunoblotting. Band intensities were analyzed by ImageJ and the MK2/Tubulin ratios in UV30-treated cells were represented in the histogram. Data represents mean ± SEM of three independent experiments. **(B)** WT and p38α KO cancer-associated fibroblasts (CAFs) were transfected with siRNA control or against MDM2, and were analyzed by immunoblotting. The histogram represents the MK2/Tubulin ratios determined as in (**A**). Data represents mean ± SEM of two independent experiments. **(C)** The indicated amounts of GST-MK2 protein were incubated with ubiquitin, E1, E2 (UBE2D3) and GST-MDM2 for 1 h at 37ºC. Samples incubated without ubiquitin were used as negative controls. Ubiquitinated MK2 (MK2(Ub)) was detected by immunoblotting with a MK2 antibody. The images shown are representative from two independent experiments. **(D)** MK2 residues ubiquitinated by MDM2 and the corresponding peptides, as identified by mass spectrometry. The ubiquitination ratio was calculated as the number of peptide spectrum matches (PSM) with the indicated residue ubiquitinated versus non-ubiquitinated. **(E)** MK2-ubiquitinated lysines are highlighted in orange in the context of the p38α-MK2 complex (PDB ID: 2OZA). The image was produced using PyMOL v2.0. **(F)** Purified GST-MK2 and GST-MK2 4K/R proteins

(2 μg) were incubated with ubiquitin, E1, E2 (UBE2D3) and GST-MDM2 for 1 h at 37ºC. Samples incubated without ubiquitin were used as negative controls. Ubiquitinated MK2 (MK2(Ub)) was detected by immunoblotting with a MK2 antibody. The images shown are representative from two independent experiments.

Fig. 7. MK2 activity modulates cell survival in response to stress. **(A)** MK2 KO MEFs were electroporated with either MK2 WT or the mutant 4K/R (K188R, K371R, K374R and K385R), stimulated with UV-C, 30 J/m^2 (UV30), and then incubated for 5 and 8 h. Cell lysates were analyzed by immunoblotting. **(B)** MEFs expressing MK2 WT or MK2 4K/R were stimulated with UV30, and then were incubated for 16 h. Cell death was analyzed by DAPI staining and normalized to the value observed in UV30-treated MK2 WT cells at 16 h. Data represents mean ± SEM of two independent experiments. **(C)** U2OS cells were pretreated with the p38α inhibitor PH797804 (p38 inh, 2 μM) and the MK2 inhibitors PF3644022 (PF, 2.5 μM) and MK2 inhibitor III (10 μM) or vehicle (DMSO) for 4 h, and then were exposed to UV30. After 24 h, cells were harvested and stained with DAPI to analyze cell death by FACS. Data was normalized to the cell death observed in UV30-treated DMSO cells. Data represents mean ± SEM of four independent experiments. **(D)** U2OS cells were pre-treated with PH797804 (p38 inh) or DMSO (-) for 2 h, treated with UV30 and then incubated for the indicated times. Cell lysates were analyzed by immunoblotting.

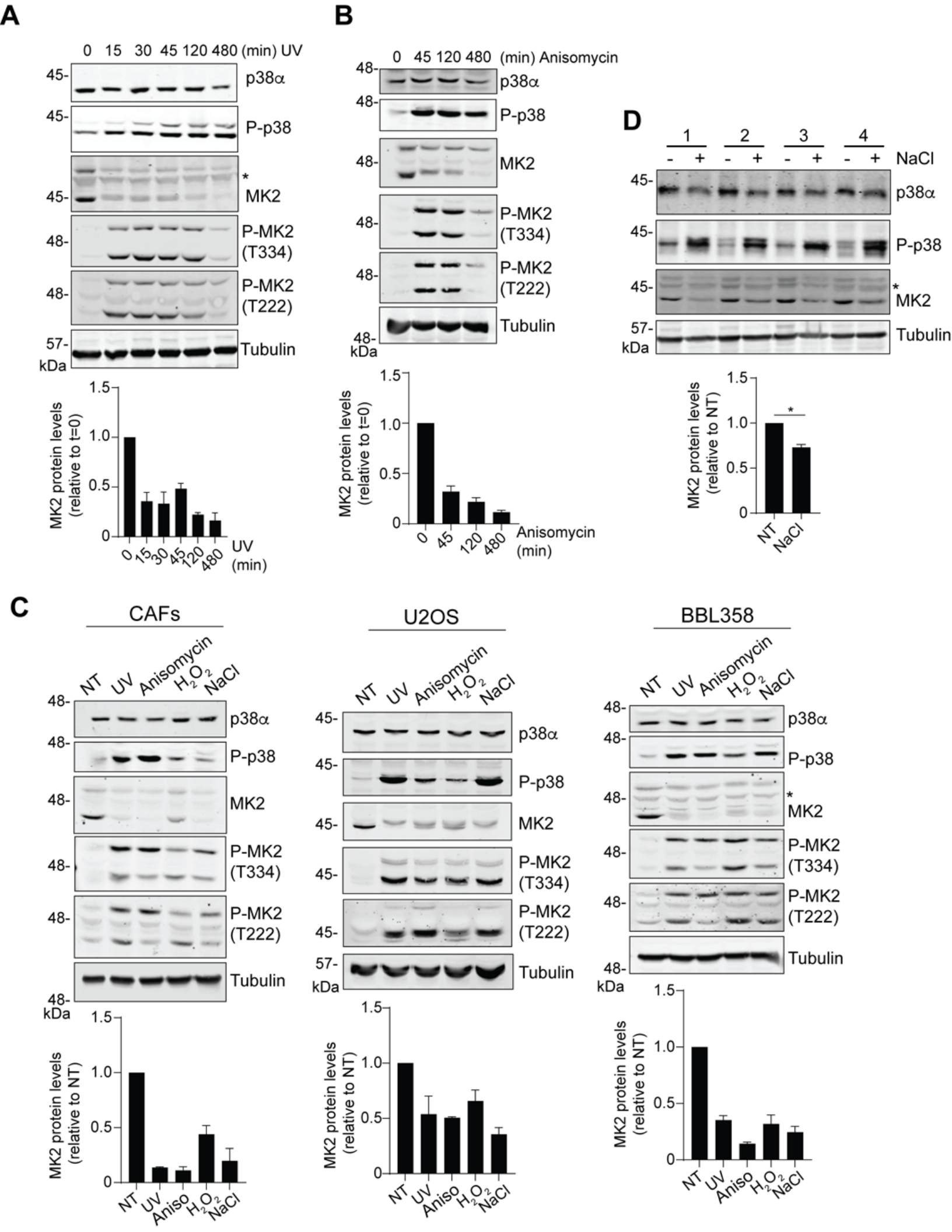
A
0 15 30 45 120 480 (min) UV
45-
p38α
45-
P-p38
45-
*
MK2
48-
P-MK2 (T334)
48-
P-MK2 (T222)
57-
kDa
Tubulin
MK2 protein levels (relative to t=0)
1.5
1.0
0.5
0
0 15 30 45 120 480
UV (min)
B
0 45 120 480 (min) Anisomycin
48-
p38α
48-
P-p38
48-
MK2
48-
P-MK2 (T334)
48-
P-MK2 (T222)
48-
kDa
Tubulin
MK2 protein levels (relative to t=0)
1.5
1.0
0.5
0
0 45 120 480
Anisomycin (min)
D
1 2 3 4
- + - + - + - + NaCl
45-
p38α
45-
P-p38
45-
*
MK2
57-
kDa
Tubulin
MK2 protein levels (relative to NT)
1.5
1.0
0.5
0
*
NT
NaCl
C
CAFs
U2OS
BBL358
NT UV Anisomycin H2O2 NaCl
48-
45-
p38α
P-p38
MK2
P-MK2 (T334)
P-MK2 (T222)
Tubulin
kDa
MK2 protein levels (relative to NT)
1.5
1.0
0.5
0
NT UV Aniso H2O2 NaCl

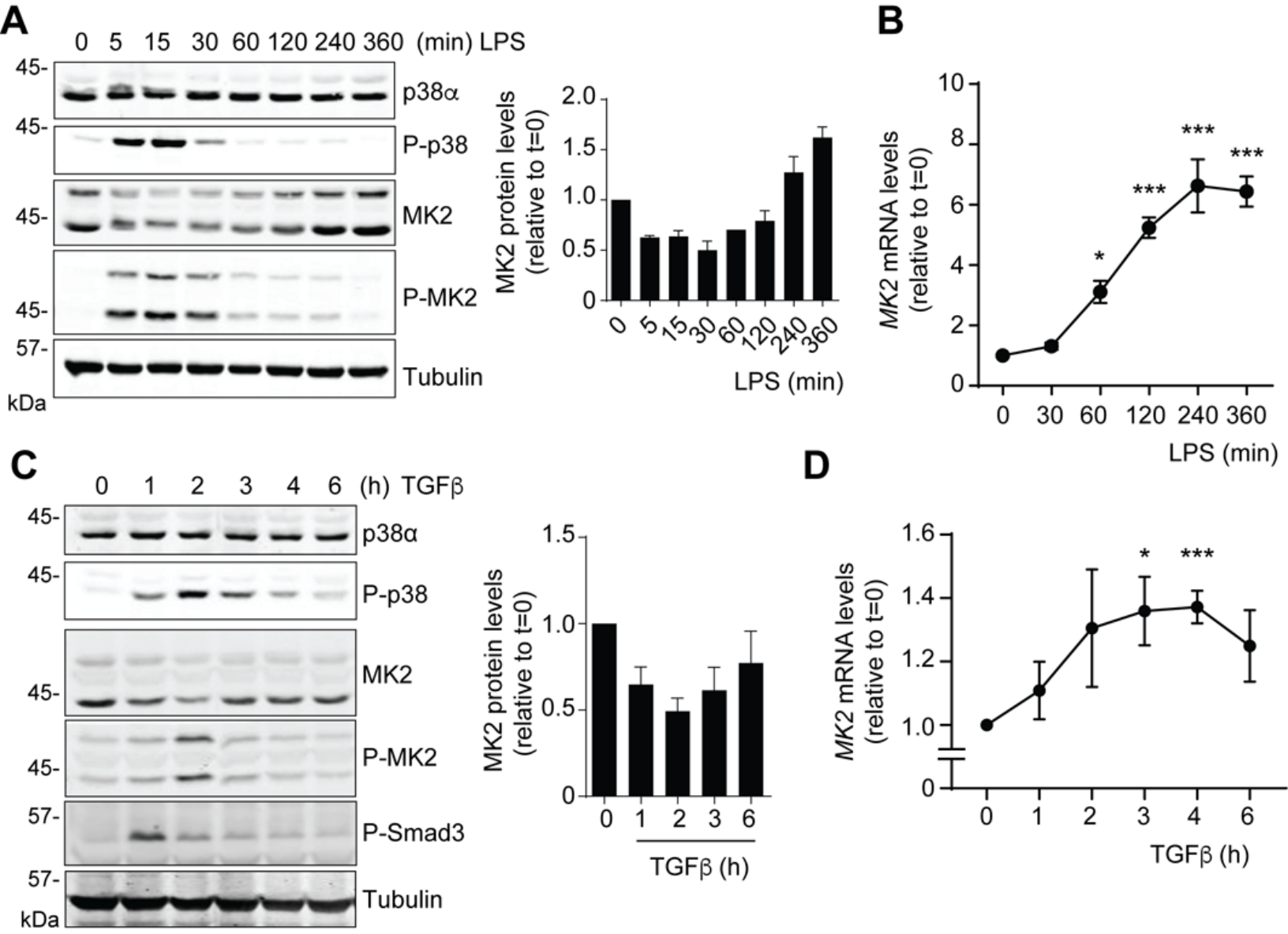
A
0 5 15 30 60 120 240 360 (min) LPS
45-
p38α
45-
P-p38
45-
MK2
P-MK2
45-
57-
Tubulin
kDa
MK2 protein levels (relative to t=0)
2.0
1.5
1.0
0.5
0
0 5 15 30 60 120 240 360
LPS (min)
B
MK2 mRNA levels (relative to t=0)
10
8
6
4
2
0
*
***
***
***
0 30 60 120 240 360
LPS (min)
C
0 1 2 3 4 6 (h) TGFβ
45-
p38α
45-
P-p38
MK2
45-
P-MK2
45-
57-
P-Smad3
57-
Tubulin
kDa
MK2 protein levels (relative to t=0)
1.5
1.0
0.5
0
0 1 2 3 6
TGFβ (h)
D
MK2 mRNA levels (relative to t=0)
1.6
1.4
1.2
1.0
0
*
***
0 1 2 3 4 6
TGFβ (h)

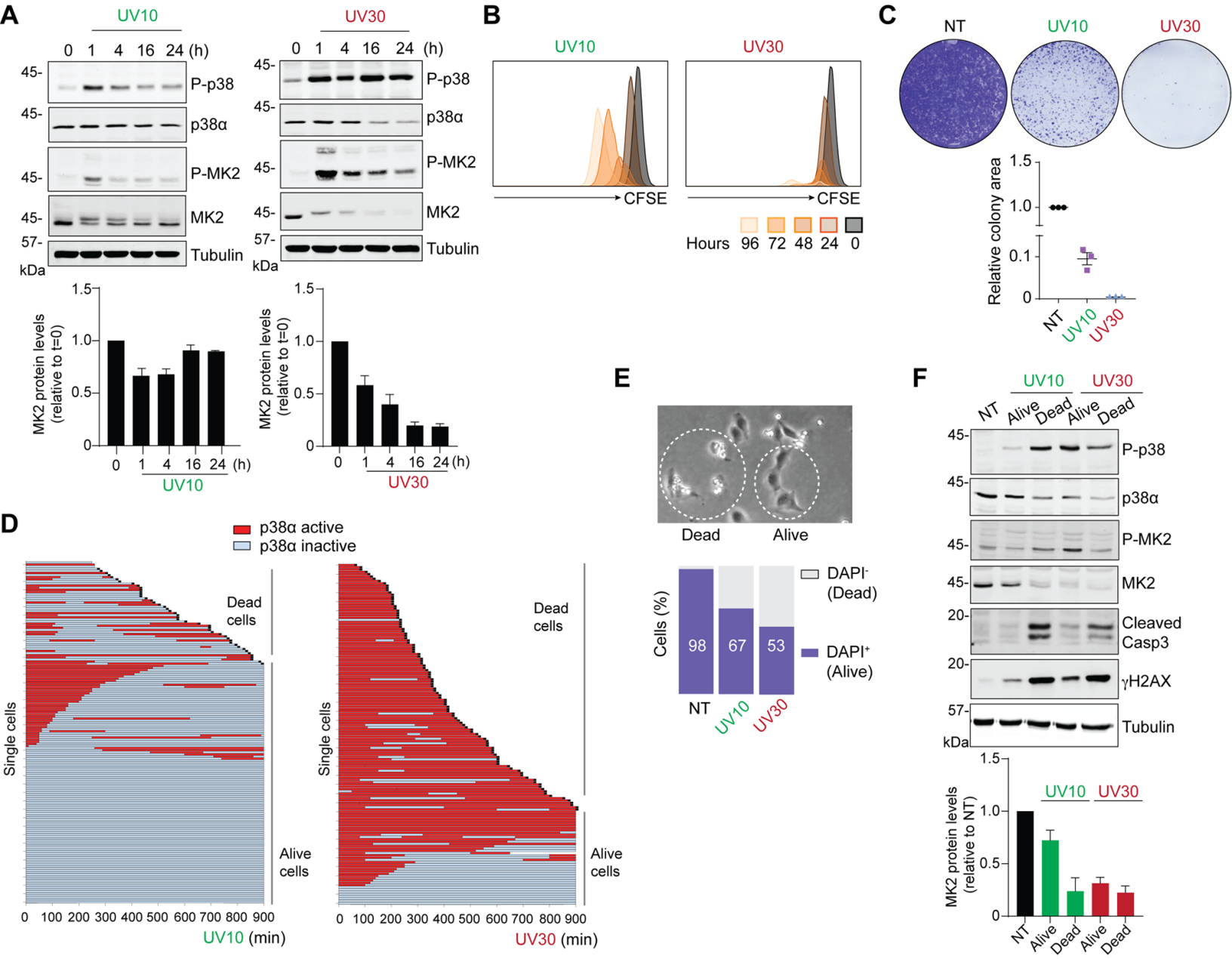
A
UV10
UV30
0 1 4 16 24 (h)
P-p38
p38α
P-MK2
MK2
Tubulin
kDa
MK2 protein levels (relative to t=0)
B
UV10
UV30
CFSE
Hours 96 72 48 24 0
C
NT
UV10
UV30
Relative colony area
D
p38α active
p38α inactive
Dead cells
Alive cells
Single cells
UV10 (min)
UV30 (min)
E
Dead
Alive
Cells (%)
98
67
53
DAPI- (Dead)
DAPI+ (Alive)
F
NT
Alive
Dead
Cleaved Casp3
γH2AX
MK2 protein levels (relative to NT)

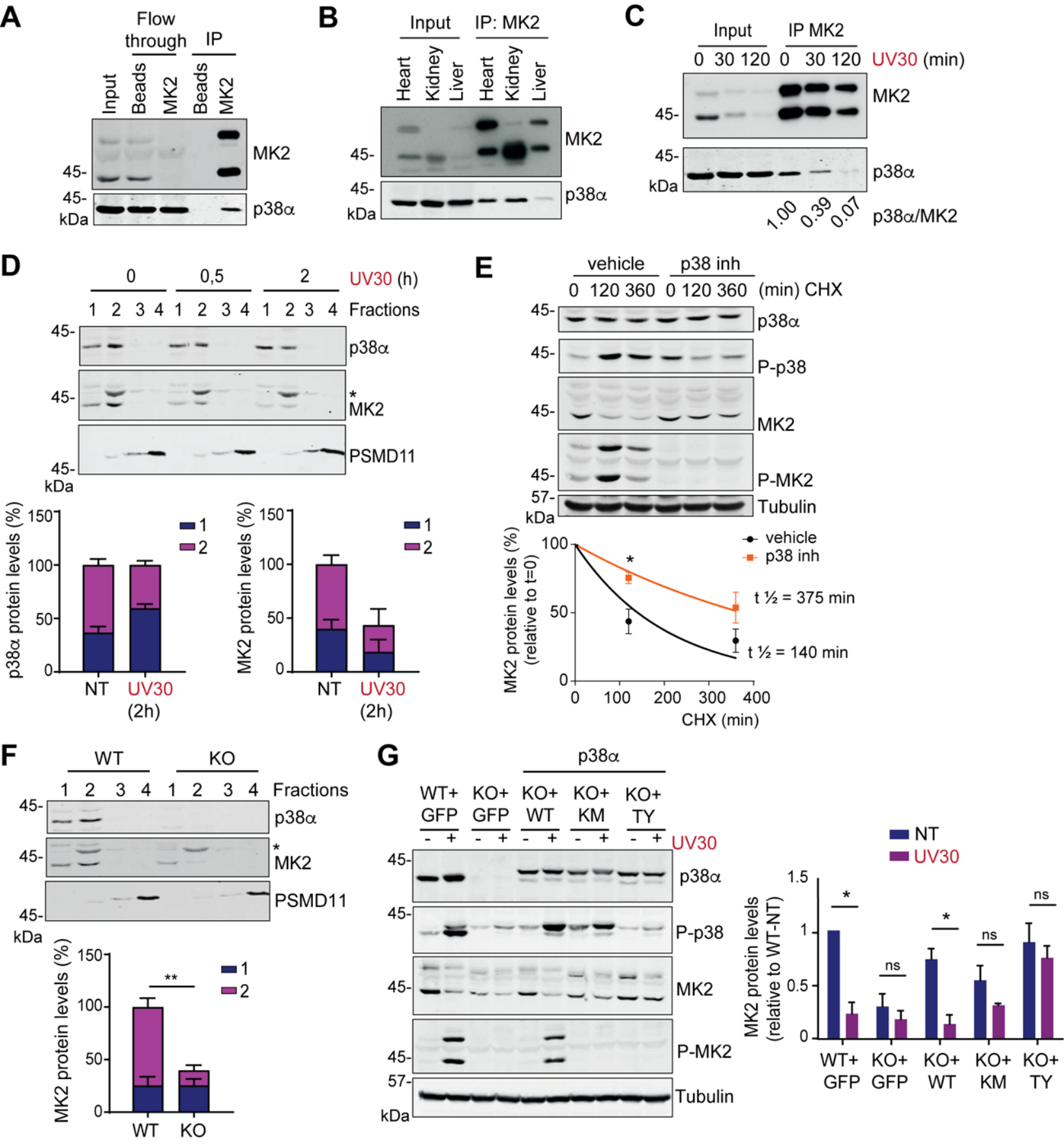
A
Flow through
IP
Input
Beads
MK2
Beads
MK2
45-
MK2
45-
kDa
p38α
B
Input
IP: MK2
Heart
Kidney
Liver
Heart
Kidney
Liver
45-
MK2
45-
kDa
p38α
C
Input
IP MK2
0 30 120 0 30 120 UV30 (min)
45-
MK2
45-
kDa
p38α
1.00 0.39 0.07
p38α/MK2
D
0
0,5
2
UV30 (h)
1 2 3 4 1 2 3 4 1 2 3 4 Fractions
45-
p38α
45-
*
MK2
PSMD11
45-
kDa
p38α protein levels (%)
150
100
50
0
1
2
NT
UV30
(2h)
MK2 protein levels (%)
150
100
50
0
1
2
NT
UV30
(2h)
E
vehicle
p38 inh
0 120 360 0 120 360 (min) CHX
45-
p38α
45-
P-p38
45-
MK2
45-
P-MK2
57-
Tubulin
kDa
MK2 protein levels (%)
(relative to t=0)
100
50
0
vehicle
p38 inh
*
t ½ = 375 min
t ½ = 140 min
0
100
200
300
400
CHX (min)
F
WT
KO
1 2 3 4 1 2 3 4 Fractions
45-
p38α
45-
*
MK2
45-
PSMD11
kDa
MK2 protein levels (%)
150
100
50
0
**
1
2
WT
KO
G
p38α
WT+ GFP
KO+ GFP
KO+ WT
KO+ KM
KO+ TY
- + - + - + - + - +
UV30
45-
p38α
45-
P-p38
45-
MK2
45-
P-MK2
57-
Tubulin
kDa
NT
UV30
MK2 protein levels
(relative to WT-NT)
1.5
1
0.5
0
*
ns
*
ns
ns
WT+ GFP
KO+ GFP
KO+ WT
KO+ KM
KO+ TY

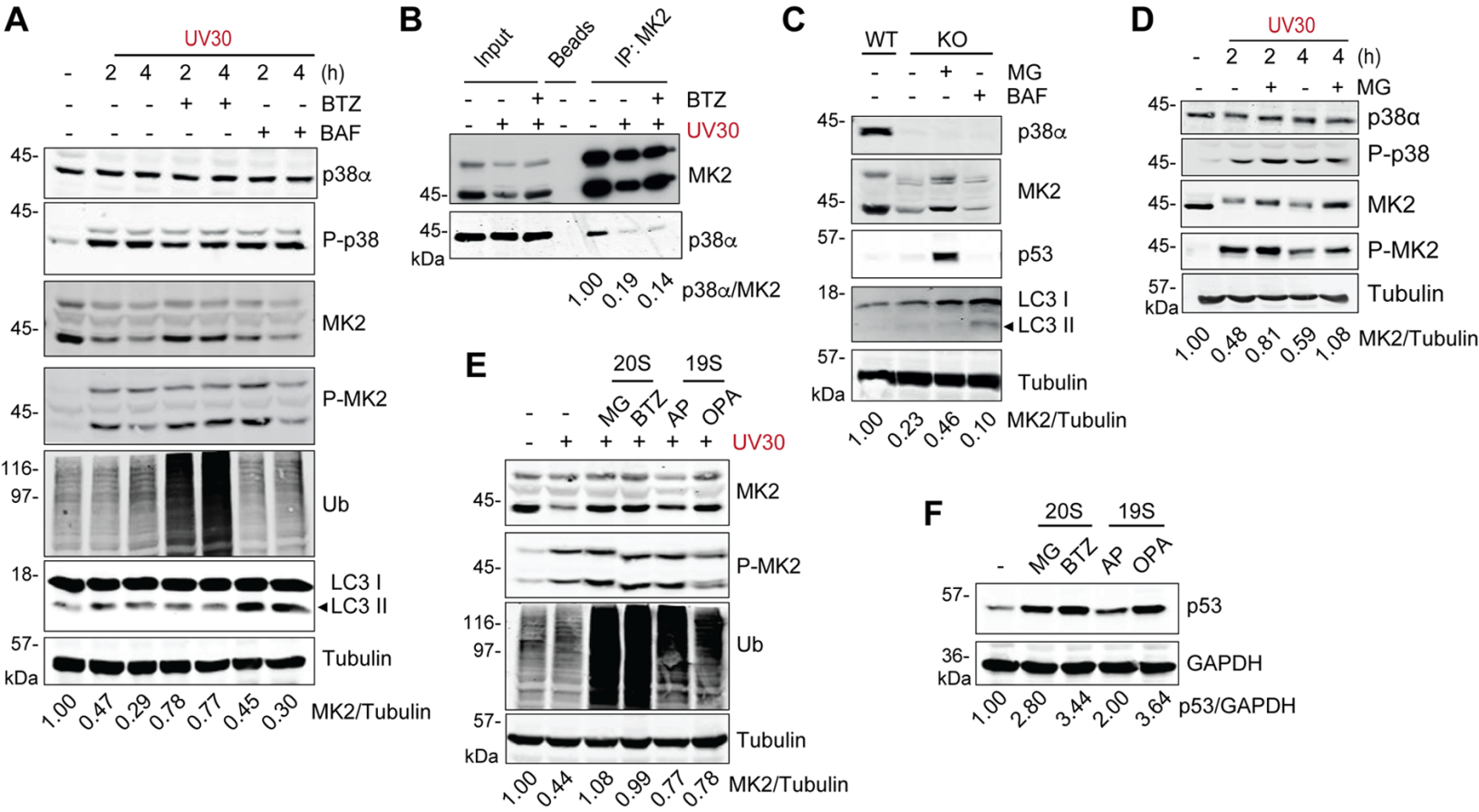
A
UV30
- 2 4 2 4 2 4 (h)
- - - + + - - BTZ
- - - - - + + BAF
45-
p38α
45-
P-p38
45-
MK2
45-
P-MK2
116-
97-
Ub
18-
LC3 I
LC3 II
57-
kDa
Tubulin
1.00 0.47 0.29 0.78 0.77 0.45 0.30 MK2/Tubulin
B
Input
Beads
IP: MK2
- - + - - - + BTZ
- + + - - + + UV30
45-
MK2
45-
kDa
p38α
1.00 0.19 0.14 p38α/MK2
C
WT
KO
- - + - MG
- - - + BAF
45-
p38α
45-
MK2
57-
p53
18-
LC3 I
LC3 II
57-
kDa
Tubulin
1.00 0.23 0.46 0.10 MK2/Tubulin
D
UV30
- 2 2 4 4 (h)
- - + - + MG
45-
p38α
45-
P-p38
45-
MK2
45-
P-MK2
57-
kDa
Tubulin
1.00 0.48 0.81 0.59 1.08 MK2/Tubulin
E
20S
19S
- - MG BTZ AP OPA
- + + + + + UV30
45-
MK2
45-
P-MK2
116-
97-
Ub
57-
kDa
Tubulin
1.00 0.44 1.08 0.99 0.77 0.78 MK2/Tubulin
F
20S
19S
- MG BTZ AP OPA
57-
p53
36-
kDa
GAPDH
1.00 2.80 3.44 2.00 3.64 p53/GAPDH

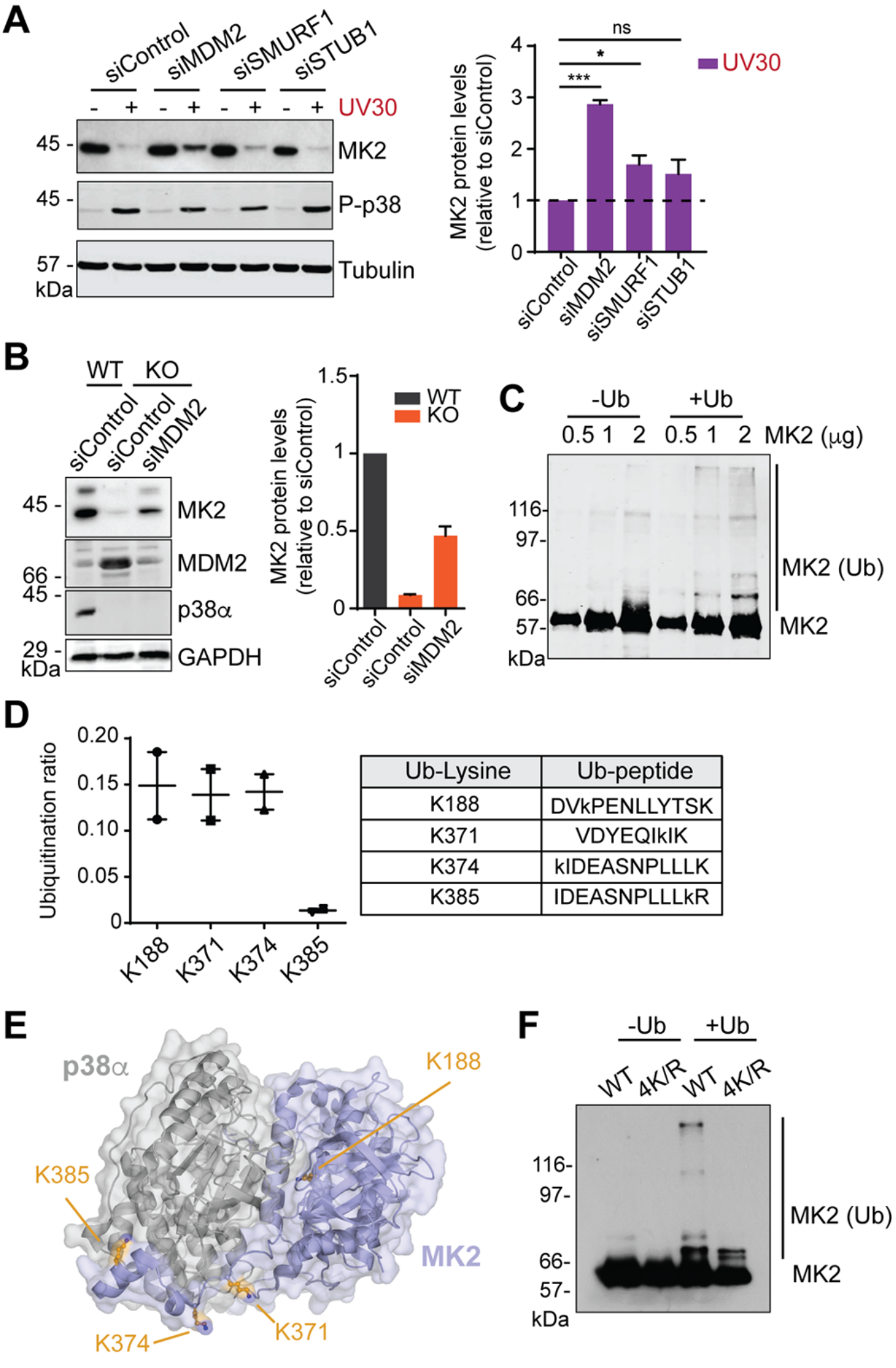
A
siControl
siMDM2
siSMURF1
siSTUB1
UV30
45 -
MK2
45 -
P-p38
57 -
kDa
Tubulin
ns
*
***
UV30
MK2 protein levels
(relative to siControl)
siControl
siMDM2
siSMURF1
siSTUB1
B
WT
KO
siControl
siControl
siMDM2
45 -
MK2
MDM2
66 -
45 -
p38α
29 -
kDa
GAPDH
WT
KO
MK2 protein levels
(relative to siControl)
siControl
siControl
siMDM2
C
-Ub
+Ub
0.5 1 2 0.5 1 2 MK2 (μg)
116-
97-
66-
57-
kDa
MK2 (Ub)
MK2
D
Ubiquitination ratio
K188
K371
K374
K385
Ub-Lysine
Ub-peptide
K188
DVkPENLLYTSK
K371
VDYEQIkIK
K374
kIDEASNPLLLK
K385
IDEASNPLLLkR
E
p38α
K188
K385
MK2
K374
K371
F
-Ub
+Ub
WT
4K/R
WT
4K/R
116-
97-
66-
57-
kDa
MK2 (Ub)
MK2

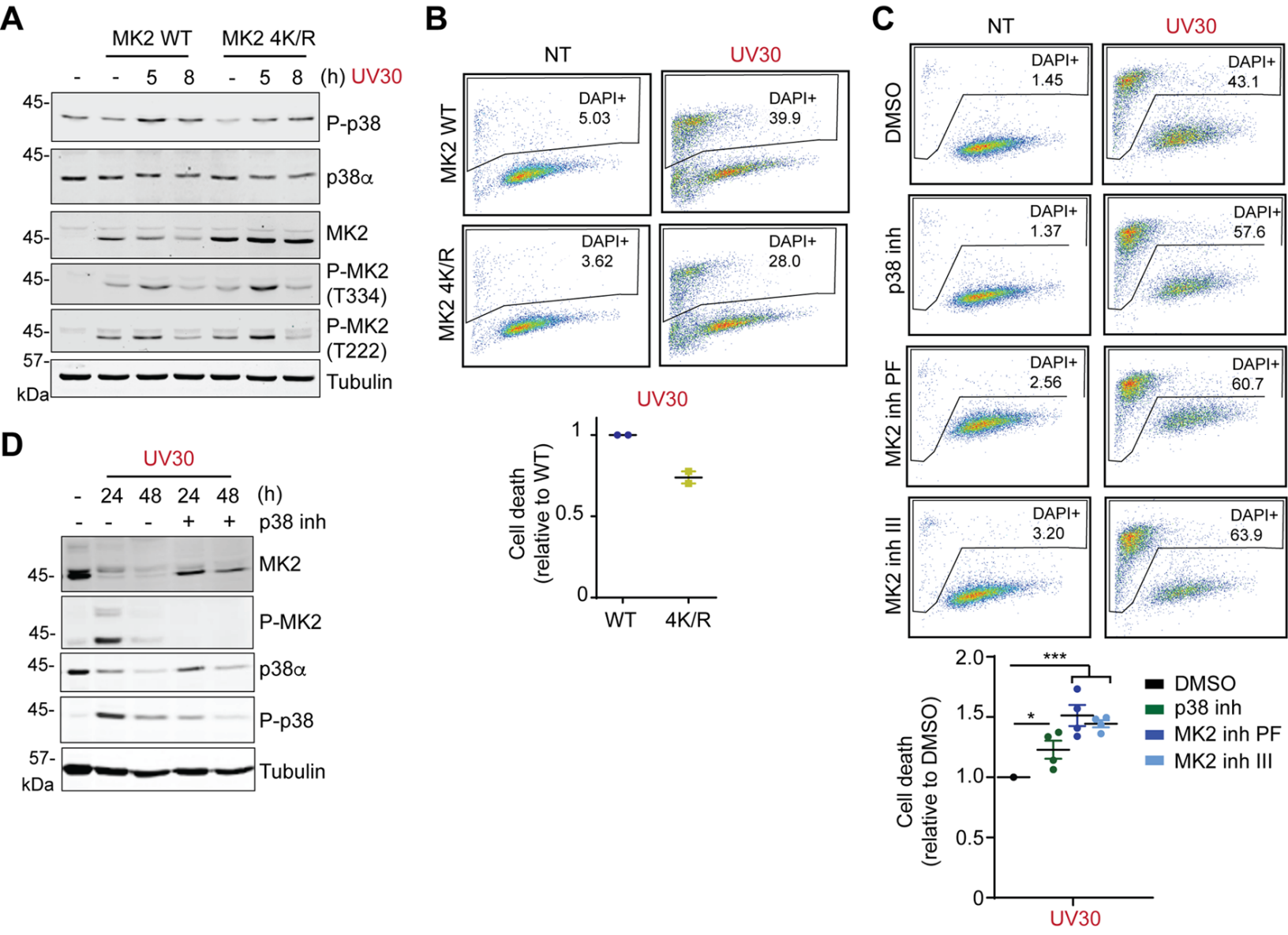
A
MK2 WT
MK2 4K/R
- - 5 8 - 5 8 (h) UV30
45-
P-p38
p38α
MK2
P-MK2 (T334)
P-MK2 (T222)
57-
Tubulin
kDa
B
NT
UV30
MK2 WT
MK2 4K/R
DAPI+ 5.03
DAPI+ 39.9
DAPI+ 3.62
DAPI+ 28.0
UV30
Cell death (relative to WT)
1
0.5
0
WT
4K/R
C
NT
UV30
DMSO
p38 inh
MK2 inh PF
MK2 inh III
DAPI+ 1.45
DAPI+ 43.1
DAPI+ 1.37
DAPI+ 57.6
DAPI+ 2.56
DAPI+ 60.7
DAPI+ 3.20
DAPI+ 63.9
Cell death (relative to DMSO)
2.0
1.5
1.0
0.5
0
***
*
DMSO
p38 inh
MK2 inh PF
MK2 inh III
UV30
D
UV30
- 24 48 24 48 (h)
- - - + + p38 inh
45-
MK2
P-MK2
p38α
P-p38
57-
Tubulin
kDa

PNAS
www.pnas.org

Supplementary Information for

MK2 degradation as a sensor of signal intensity that controls stress-induced cell fate

Nuria Gutierrez-Prat, Monica Cubillos-Rojas, Begoña Cánovas, Antonija Kuzmanic, Jalaj Gupta, Ana Igea, Elisabet Llonch, Matthias Gaestel, and Angel R. Nebreda

Corresponding author: Angel R. Nebreda
Email: angel.nebreda@irbbarcelona.org

This PDF file includes:

Supplementary Methods

Cell culture. The following cells were used in this study: cancer-associated fibroblasts (CAFs), bone marrow derived macrophages (BMDMs), colon fibroblasts, mesenchymal stem cells (MSCs), mouse embryonic fibroblasts (MEFs), BBL358 epithelial cancer cells, and the cell lines U2OS and HEK293T. To generate CAFs, mammary tumors induced by MMTV-PyMT expression in *Mapk14*$^{lox/lox}$ UBC-Cre-ERT2 female mice (1) were chopped using razors and digested at 37°C rocking for 1 h in supplemented Dulbecco's modified Eagle medium (DMEM, Sigma, D5796) with 10% fetal bovine serum (FBS, Termo Scientifc, E6541L), 2 mM L-Glutamine (LabClinics, M11–004), 100 μg/ml penicillin-streptomycin (LabClinics, P11-010), 1 mg/ml Collagenase A (Roche #10103586001) and 1.5 units/ml Hyaluronidase (Sigma, #H3506). After digestion, the cell suspension was filtered through a 70 μm cell strainer and centrifuged for 5 min at 1500 rpm. The cell pellet was resuspended in 10 ml of supplemented DMEM and centrifuged at 1500 rpm for 30 s. The supernatant was discarded, and the cell pellet was resuspended and spun again four more times before plating. Cells were passaged until spontaneously immortalized. Immortalized cells were stained with propidium iodide (PI) and PDGFα^{+} (ebiosciences, #12-1401-81, 1:100), EpCAM^{-} (Santa Cruz, #sc-53532, 1:200), CD45^{-} (BD Biosciences, #550539, 1:200) and PI^{-} cells were sorted in a FACS Aria flow cytometer (BD Biosciences). BMDMs were generated from bone marrow precursor cells isolated from femurs and tibias of mice by incubation in conditioned media from the mouse fibroblast cell line L929 (L-cell) for 6 days, and then were cultured in complete DMEM as described (2). Colon fibroblasts were isolated from *Mapk14*$^{lox/lox}$ UBC-Cre-ERT2 mice. Colons were dissected, opened longitudinally and washed with cold PBS, incubated with 8 mM EDTA at 37ºC for 15 min. Supernatants were centrifuged at 1200 rpm for 5 min at 4ºC, and pelleted cells were digested with Dispase II (0.5 mg/ml, Roche #04942078001) at 37ºC for 25 min to isolate epithelial cells. To obtain lamina propria (mesenchymal and leucocytes cells) colon pieces were collected, cut (2-3 mm) and digested with mix of collagenase A (1.75 mg/ml, Roche #10103586001) at 37ºC for 45 min. Cells were sorted in a FACS Aria flow cytometer (BD Biosciences) using CD45- (BD Biosciences, #550539, 1:200), CD31- (Abcam, # ab28364, 1:500), CD140a+ (Ebiosciences, #12-1401-81, 1:100) and CD140b+ (Ebioscience #17-1402-82, 1:25). MSCs were obtained from mice as described (3). MK2 KO MEFs were generated as reported (4). BBL358 epithelial cancer cells

were obtained from PyMT-induced mammary tumors (1). U2OS and HEK293T cells were purchased from ATCC. All cells were cultured in DMEM supplemented with 10% FBS, 1 % L-Glutamine and 1% penicillin-streptomycin at 37ºC and 5% CO_2. For passaging, cells were washed in PBS and incubated in 1 ml trypsin at 37ºC until detached. Then, complete media was added, and cells were diluted as desired depending on the confluence and re-plated in a new culture dish. Differentiated BMDMs were harvested by using cell scrappers and plated with the same media until they attached. Before LPS treatment, BMDMs were incubated for 18 h in DMEM (10% FBS, 1% P/S) without L-cell conditioned media to render cells quiescent and synchronize the culture.

DAPI staining. U2OS cells were harvested, washed in PBS and incubated with DAPI for 10 min at RT. Cells were subjected to FACS analysis and analyzed using FlowJo software.

Retrovirus production, cell infection and electroporation. For retrovirus production, HEK293T were transiently co-transfected with 5 μg of pBabe-puro vector containing the different p38α mutants and 5 μg of the pCL-Eco packaging plasmid using the calcium chloride method. After overnight, the media was replaced, and 48 h later, the virus-containing media was collected and passed through PVDF filters. For cell infection, the virus-containing media was diluted 1:2 in buffer with 8 μg/ml of polybrene and added to the cell monolayer. The following day media was replaced, and 24 h later the cells started to be selected with puromycin (1 μg/ml) for 24-48 h. Selected cell populations were cultured in puromycin-containing media (1 μg/ml).

WT and p38α KO CAFs were infected with retroviruses that express p38α WT, or the mutants with Lys53 changed to Met (KM), or with Thr180 and Tyr182 mutated to Ala and Phe, respectively (TY). GFP-expressing retroviruses were used as control. U2OS cells expressing p38α-KTR were generated using viral constructions previously described (5). MK2 KO MEFs (4) were electroporated with either MK2 WT or the mutant MK2 4K/R (K188R, K371R, K374R and K385R) using the MEF Starter Nucleofector Kit (Lonza, #V4XP-4012) following the manufacturer's protocol. Briefly, $8x10^6$ cells were electroporated with 1 pulse of 1350V during 30 ms and plated in a 10 cm plate. The MK2 4K/R mutant was generated by introducing a truncated form of MK2 lacking the initial 46 amino acid proline rich domain into the pGEX-KG

expression vector using Gibson assembly. The pGEX-KG vector was linearized with BamHI and HindIII, and the MK2 fragment was amplified using the primers 5'atcggatctggttccgcgtggatccatggtcaagtcgggcctgcag 3' and 5'tcagtcagtcacgatgaataagctttcgagtcagtgggcgagag 3'. Backbone and insert were assembled as described (6) using Phusion DNA polymerase.

Activation of p38α in mouse mammary tumors. Mouse mammary tumors generated by expression of the MMTV-PyMT transgene were isolated and treated with 300 mM of NaCl for 15 min. Then tumors were immersed in lysis buffer, and homogenized using Precellys homogenization and lysis instrument (Bertin Technologies). Lysates were incubated 15 min on ice and centrifuged 15 min at 13200 rpm at 4°C.

Immunoblotting. Breast tumors from MMTV-PyMT female mice and tissues from mice WT or p38α KO (1) were homogenized in 1% NP40, 150 mM NaCl, 50 mM Tris HCl pH 7.5, 2 mM EDTA, 2 mM EGTA, 20 mM Sodium fluoride, 1 mM PMSF, 2.5 mM Benzamidine, 1 mM sodium orthovanadate, 2 μM microcystin, 10 μg/ml pepstatin, 10 μg/ml leupeptin and 10 μg/ml aprotinin, using the Precellys lysis instrument (Bertin technologies). Cultured cells were lysed by scrapping in the same buffer. Protein content was quantified using the RC DC Protein Assay Kit I (Bio-Rad #5000111) with BSA as standard. Total protein lysates (50 μg) were separated on SDS-PAGE and transferred to nitrocellulose membrane (GE Healthcare life sciences # 10600001). After blocking (5% non-fat milk and 1% BSA in PBS, 1 h at RT) membranes were incubated at 4ºC overnight with primary antibodies. The following antibodies were used: p38α (Santa Cruz, #sc-535-G, 1:1000), phospho-Thr180/Tyr182 p38 (Cell Signaling, #9211S, 1:1000), phospho-Thr180/Tyr182 p38 (BD Biosciences # 612288, 1:1000), p53 (Cell Signaling #2524S, 1:1000), phospho-Ser423/425 Smad 3 (Cell Signaling, # 9520S), mono- and polyubiquitinylated conjugates (Enzo life science #BML-PW8810-0100, 1:1000), LC3 (BioNova cientifica #PM036, 1:1000), MK2 (Cell Signaling, #3042 1:500), phospho-Thr 334 MK2 (Cell Signaling, #3007, 1:500), phospho-Thr 222 MK2 (Cell Signaling #3316, 1:500), MDM2 (Santa Cruz, sc-965), PSMD11 (Cell Signaling, 14303S), H2AX Phospho S139 (Millipore, #05-636) and Caspase 3 (Cell Signaling, #9662S). Tubulin (Sigma, #T9026) and GAPDH (Sigma, #G8795) were used at 1:5000 as loading controls. Secondary Alexa Fluor-conjugated antibodies were diluted 1:5000 in

1% non-fatty milk. Membranes were analyzed using the Odyssey Infrared Imaging System (Li-Cor Biosciences). Densitometric quantifications were performed using ImageJ software.

Analysis of mRNA expression. Total RNA was extracted from cells using TRIzol (Invitrogen) or a RNA mini kit (Ambion) following the manufacturer's instructions. To determine RNA concentrations, the absorbance at 260 nm was measured by Nanodrop. cDNA was obtained from 1 μg of purified RNA using SuperScript IV Reverse Transcriptase (Invitrogen) in a final volume of 10 μl. For RT-PCR, 4.6 μl of cDNA (5 ng/reaction) were loaded in triplicates in a 384 well plate and 5.4 μl of the mix reaction were added. The plate was sealed and centrifuged for 1 min at 200 xg and run as follows: 50 °C for 2 min, 95 °C for 10 min, 40 cycles of denaturation at 95 °C for 15 s, annealing and elongation at 60 °C for 1 min, and three final steps of 95 °C for 15 s, 60 °C for 1min and 95 °C for 15 s. GAPDH was used as a reference and the ΔΔC(t) method was used to quantify gene expression. The following primers were used: MK2: 5' gtcagaagtatcagaagaagtg 3' and 5' ggttcatgaattctgtgatgg 3', SMURF1 5'gagagcttcgatgaagaaag 3'and 5' gaatgtcgatccggttaaag 3'; STUB1 5' tggaacagcattgaggag 3' and 5' atgtacttgtcgtgcttg 3'; MDM2 5' tgaggagcaggcaaatg 3' and 5'gtctaaccagggtctcttg 3'. GAPDH 5'cttcaccaccatggaggaggc 3'; 5'ggcatggactgtggtcatgag 3'.

Mass spectrometry analysis. Samples were reduced with DTT, carbamidomethylated and digested with trypsin (2% w) following FASP protocol [Wiśniewski, 2009 #113]. Digested samples were evaporated to dry and reconstituted in 14 μL of 3% ACN/1% formic acid aqueous solution. The nano-LC-MS/MS set up was as follows. Digested peptides were diluted in 3% ACN/1% FA. Sample was loaded to a 300 μm × 5 mm PepMap100, 5 μm, 100 Å, C18 μ-precolumn at a flow rate of 15 μl/min using a Thermo Scientific Dionex Ultimate 3000 chromatographic system. Peptides were separated using a C18 analytical column Acclaim PepMap® RSLC (75 μm × 50 cm, nanoViper, C18, 2 μm, 100Å) with a 120 min run, comprising three consecutive steps with linear gradients from 3 to 35% B in 90 min, from 35 to 50% B in 5 min, and from 50 % to 85 % B in 2 min, followed by isocratic elution at 85 % B in 5 min and stabilization to initial conditions (A= 0.1% FA in water, B= 0.1% FA in CH3CN). The column outlet was directly connected to an Advion TriVersa NanoMate fitted on an Orbitrap Fusion Lumos™ Tribrid. The mass spectrometer was operated in a data-dependent acquisition (DDA)

mode. Survey MS scans were acquired in the Orbitrap with the resolution (defined at 200 m/z) set to 120,000. The lock mass was user-defined at 445.12 m/z in each Orbitrap scan. The top speed (most intense) ions per scan were fragmented by HCD and detected in the orbitrap. The ion count target value was 400,000 and 10,000 for the survey scan and for the MS/MS scan respectively. Target ions already selected for MS/MS were dynamically excluded for 15s. Spray voltage in the NanoMate source was set to 1.60 kV. RF Lens were tuned to 30%. Minimal signal required to trigger MS to MS/MS switch was set to 25,000. The spectrometer was working in positive polarity mode and singly charge state precursors were rejected for fragmentation. A database search was performed with Proteome Discoverer software v2.3.0.480 using Sequest HT search engine and SwissProt Mouse canonical released 2019_01, contaminants database and MAPK2_HUMAN (P49137) protein manually introduced. Search was run against targeted and decoy database to determine the false discovery rate (FDR). Search parameters included trypsin enzyme specificity, allowing for two missed cleavage sites, oxidation in M, ubiquitination residue in K, acetylation in protein N-terminus as dynamic modifications and carbamidomethylation in C as static modification. Peptide mass tolerance was 10 ppm and the MS/MS tolerance was 0.02 Da. Peptides with a q-value lower than 0.1 and a FDR < 1% were considered as positive identifications with a high confidence level. Finally, the Percolator FDR node was used to estimate the number of falsely identified proteins among all the identified proteins. The ptmRS node was used to provide a confidence measure for the localization of ubiquitination in the peptide sequences identified with this modification. Peptide spectrum matches (PSM) were considered for relative quantification. Ratios of the peptides with or without ubiquitination were calculated and ubiquitination sites relative abundance was determined.

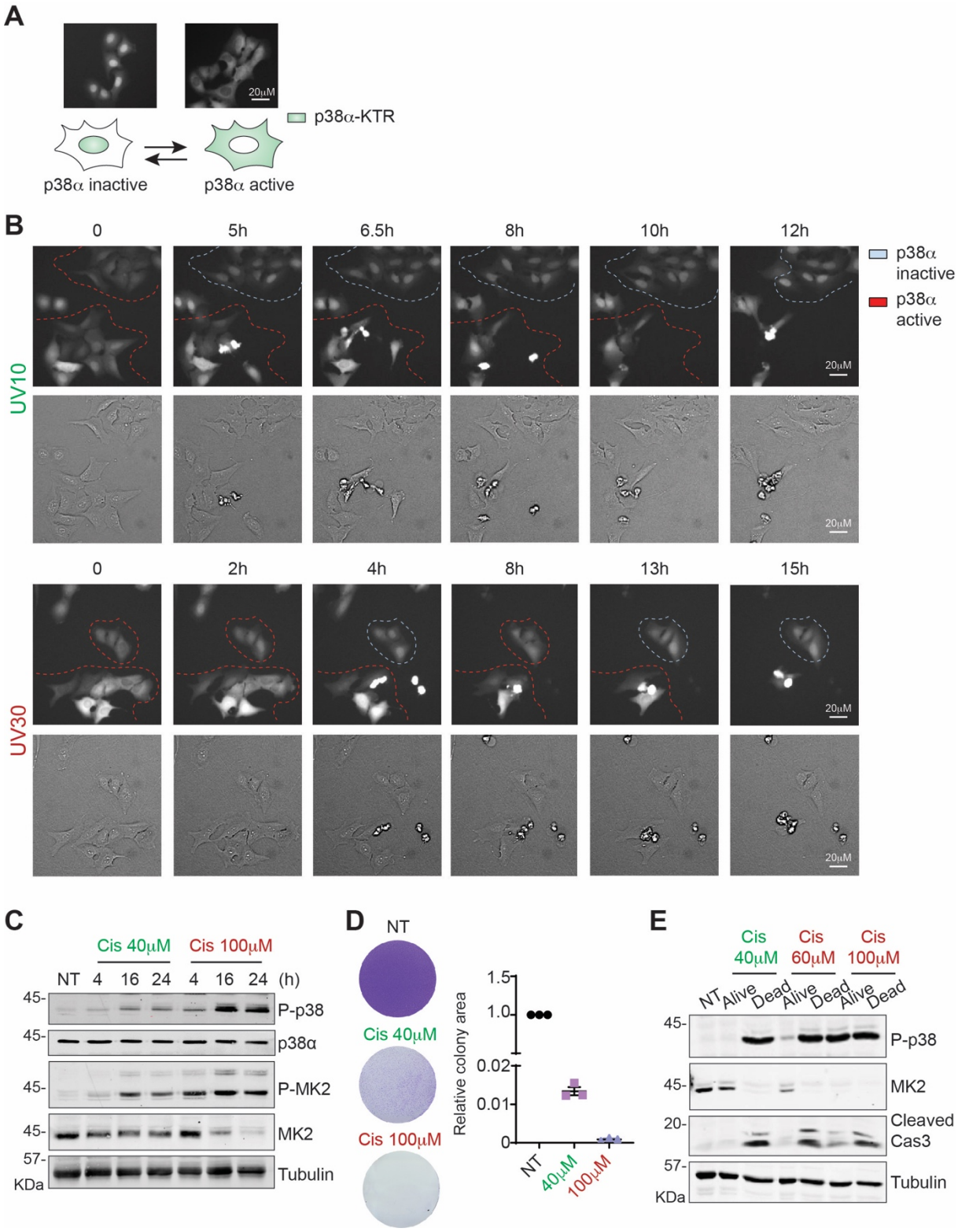

Fig. S1. MK2 levels are regulated by p38α activation and affect the stress-mediated cell outcome. **(A)** Schematic representation of the p38α-kinase translocation reporter (p38α-KTR) (5). The phosphorylation-mediated translocation of the p38α-KTR is illustrated by both cell images (upper panel) and a cartoon (lower panel). Images show U2OS cells expressing the

p38α-KTR before (left) and after (right) UV-C (30 J/m^2) stimulation. Scale bar, 20 μm. **(B)** U2OS cells expressing p38α-KTR were treated with UV-C, 10 J/m^2 (UV10) or 30 J/m^2 (UV30) (t=0) and were monitored by time-lapse microscopy every 10 min. Representative images of the time course are shown. The p38α activity status is indicated in different subset of cells enclosed by red (active) or blue (inactive) dotted lines. Scale bar, 20 μm. **(C)** U2OS cells were exposed to Cisplatin (Cis) 40 μM or 100 μM, and then were incubated for the indicated times. Cell lysates were analyzed by immunoblotting. **(D)** U2OS cells were exposed to Cis 40 μM or 100 μM or were left untreated (NT), and then were plated to form colonies, which were analyzed 7 days later. The graph shows the colony area relative to NT cells. **(E)** U2OS cells were either treated with Cis 40 μM or 100 μM, or left untreated. After 24 h, floating and poorly-attached cells (dead) were separated from the well-attached cells (alive). Lysates were prepared from the two cell populations and were analyzed by immunoblotting. Cell death was confirmed by the detection of cleaved caspase-3.

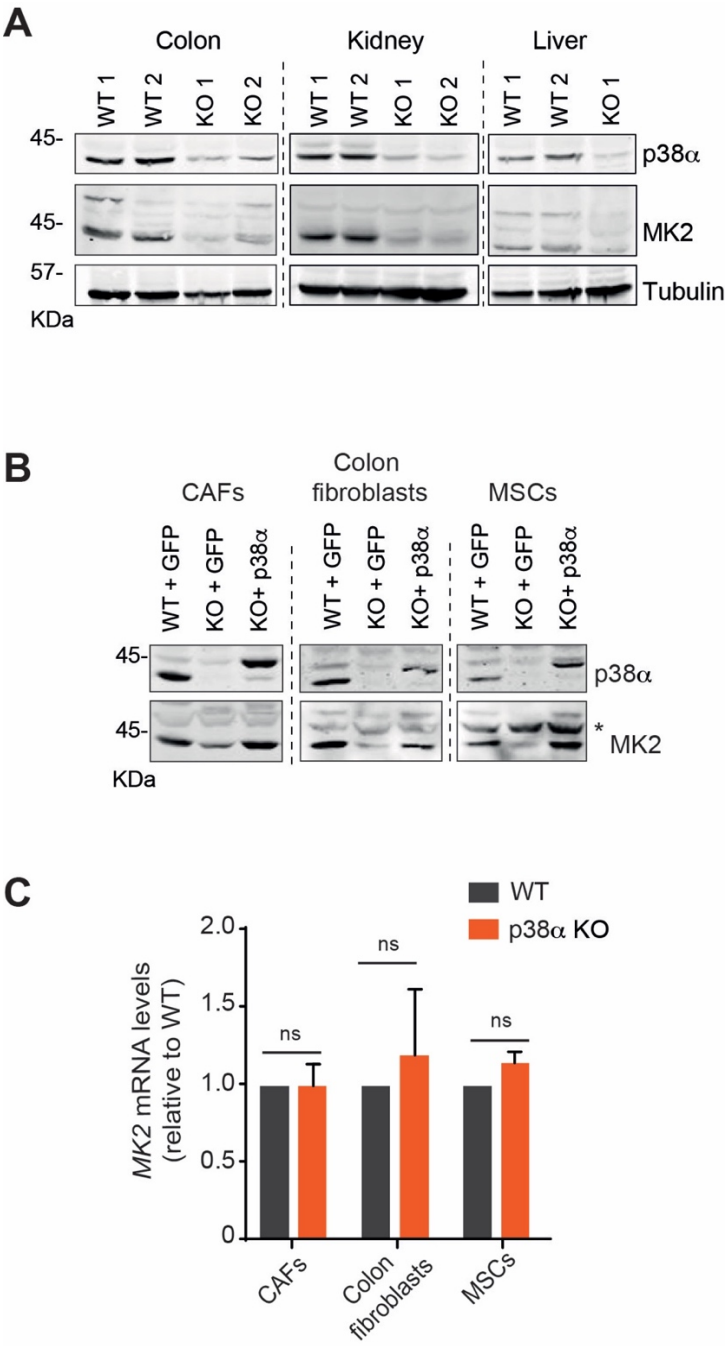

Fig. S2. p38α is required for MK2 protein accumulation. **(A)** Lysates were prepared from the indicated WT and p38α KO adult mouse tissues and were analyzed by immunoblotting. **(B)** Lysates were prepared from WT and p38α KO cancer associated fibroblasts (CAFs), colon fibroblasts and mesenchymal stem cells (MSCs), as well as from p38α KO cells re-expressing p38α or GFP, and were analyzed by immunoblotting. The asterisk indicates a non-specific band. **(C)** MK2 mRNA levels from the indicated WT and p38α KO cells were analyzed by qRT-PCR and are referred to the expression level in the WT cells which was given the value of 1. Data are mean ± SEM, n=2.

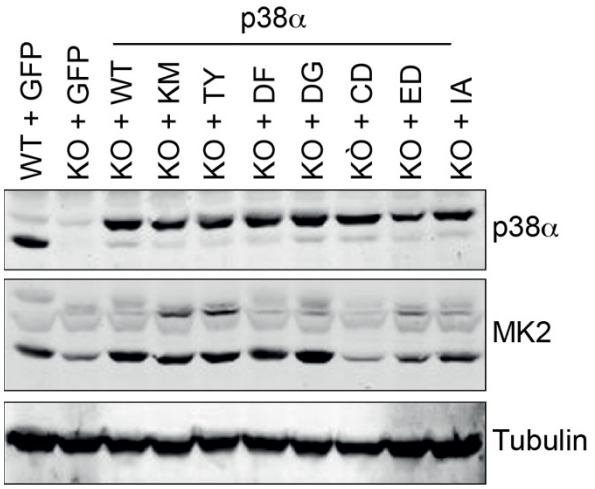

Fig. S3. The common docking of p38α is essential to stabilize MK2 protein levels. p38α KO cancer associated fibroblasts were infected with retroviruses that express p38α WT or the indicated p38α mutants, or with a vector expressing GFP. WT cells were also infected with retroviruses that express GFP. Lysates were analyzed by immunoblotting with the indicated antibodies. The p38α mutants are described in Table S1.

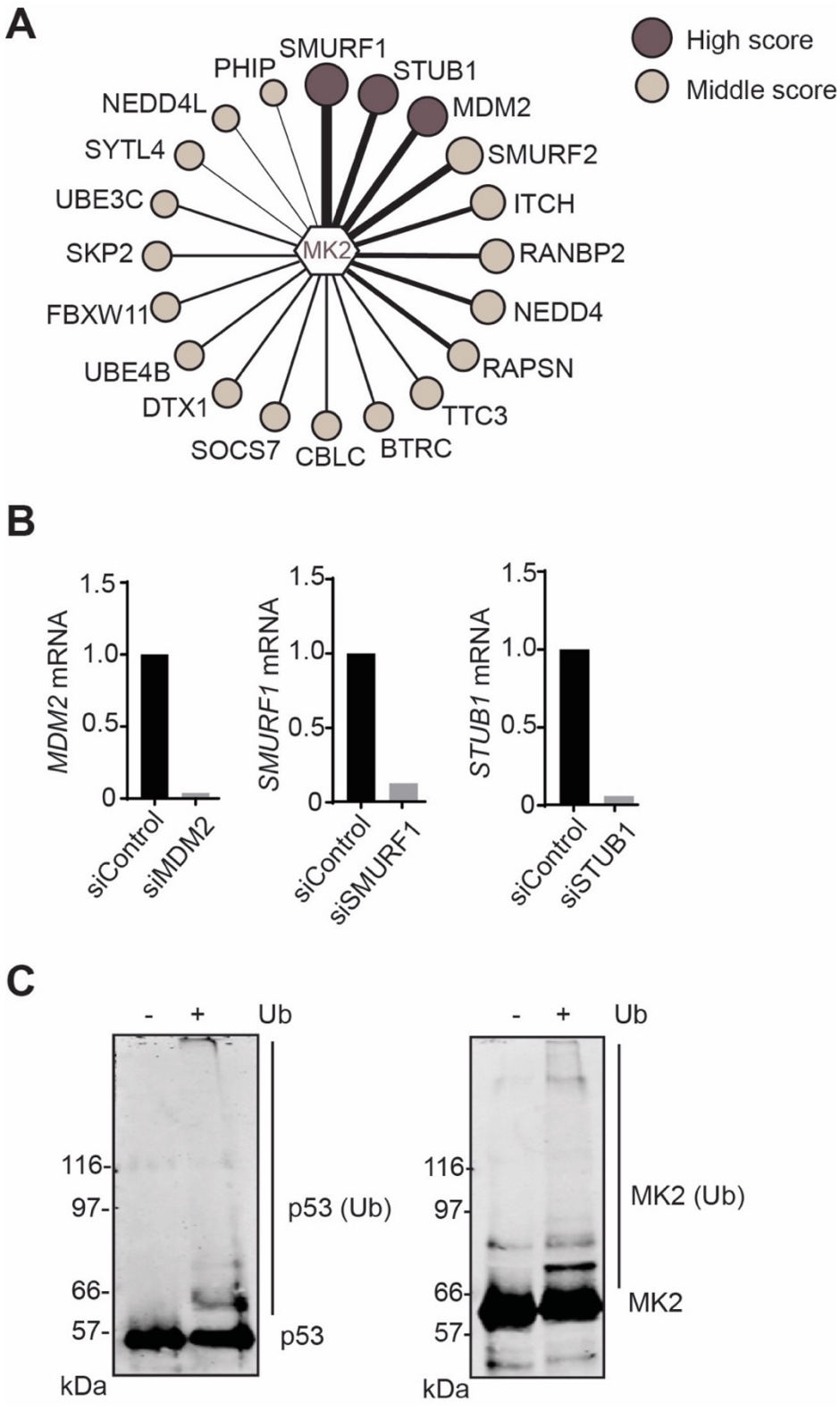

Fig. S4. Regulation of MK2 degradation by the MDM2 ubiquitin ligase. **(A)** Network view of the top 20 E3 ligases predicted to target MK2, according to the webserver http://ubibrowser.ncpsb.org. E3 ligase-MK2 interactions with a high confidence score (>0.770)

are shown darker. **(B)** U2OS cells were transfected with siRNAs against MDM2, SMURF1 and STUB1, or a non-targeting control, and the expression levels of the indicated mRNAs were determined by qRT-PCR and referred to the expression levels in siControl-treated cells. **(C)** Purified GST-p53 of GST-MK2 proteins were incubated with ubiquitin, E1, E2 (UBE2D3) and GST-MDM2 for 1 h at 37ºC. Samples incubated without ubiquitin (-) were used as negative controls. Ubiquitinated (Ub) p53 and MK2 were detected by immunoblotting.

VDYEQIkIK

#1	b	b²	Seq.	y	y²	#2
1	100.07569	50.54148	V			9
2	215.10263	108.05496	D	1150.61026	575.80877	8
3	378.16596	189.58662	Y	1035.58332	518.29530	7
4	507.20855	254.10792	E	872.51999	436.76363	6
5	635.26713	318.13720	Q	743.47740	372.24234	5
6	748.35120	374.67924	I	615.41882	308.21305	4
7	990.48909	495.74818	K-GG	502.33476	251.67102	3
8	1103.57315	552.29021	I	260.19687	130.60207	2
9			K	147.11280	74.06004	1

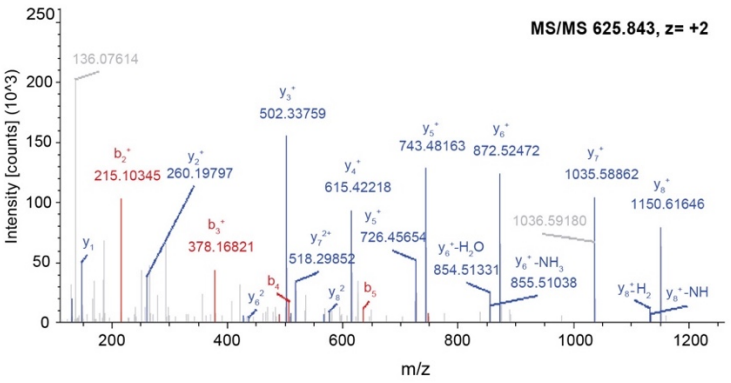

DVkPENLLYTSK

#1	b	b²	Seq.	y	y²	#2
1	116.03422	58.52075	D			12
2	215.10263	108.05496	V	1405.76856	703.38792	11
3	457.24052	229.12390	K-GG	1306.70014	653.85371	10
4	554.29329	277.65028	P	1064.56225	532.78476	9
5	683.33588	342.17158	E	967.50949	484.25838	8
6	797.37881	399.19304	N	838.46689	419.73709	7
7	910.46287	455.73507	L	724.42397	362.71562	6
8	1023.54694	512.27711	L	611.33990	306.17359	5
9	1186.61026	593.80877	Y	498.25584	249.63156	4
10	1287.65794	644.33261	T	335.19251	168.09989	3
11	1374.68997	687.84862	S	234.14483	117.57605	2
12			K	147.11280	74.06004	1

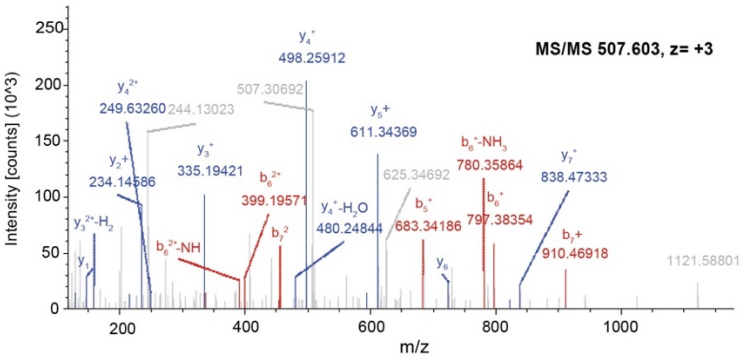

IDEASNPLLLkR

#1	b	b²	Seq.	y	y²	#2
1	114.09134	57.54931	I			12
2	243.13393	122.07061	E	1369.74340	685.37534	11
3	358.16088	179.58408	D	1240.70081	620.85404	10
4	429.19799	215.10263	A	1125.67387	563.34057	9
5	516.23002	258.61865	S	1054.63675	527.82202	8
6	630.27295	315.64011	N	967.60473	484.30600	7
7	727.32571	364.16649	P	853.56180	427.28454	6
8	840.40977	420.70853	L	756.50903	378.75816	5
9	953.49384	477.25056	L	643.42497	322.21612	4
10	1066.57790	533.79259	L	530.34091	265.67409	3
11	1308.71579	654.86153	K-GG	417.25684	209.13206	2
12			R	175.11895	88.06311	1

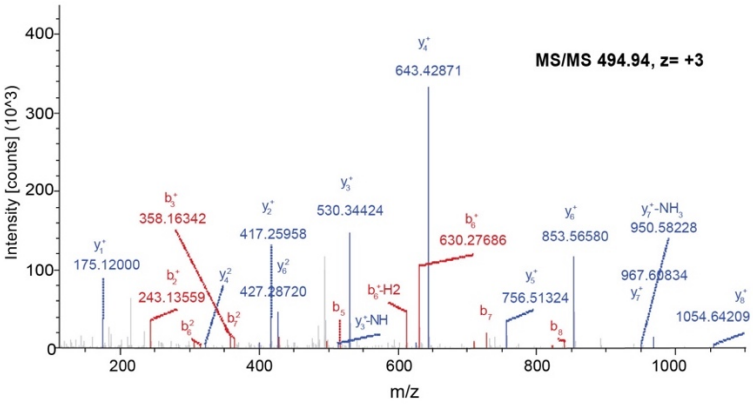

kIDEASNPLLLK

#1	b	b²	Seq.	y	y²	#2
1	243.14517	122.07622	K-GG			12
2	356.22923	178.61825	I	1212.68343	606.84535	11
3	485.27182	243.13955	E	1099.59937	550.30332	10
4	600.29877	300.65302	D	970.55677	485.78202	9
5	671.33588	336.17158	A	855.52983	428.26855	8
6	758.36791	379.68759	S	784.49272	392.75000	7
7	872.41084	436.70906	N	697.46069	349.23398	6
8	969.46360	485.23544	P	583.41776	292.21252	5
9	1082.54766	541.77747	L	486.36500	243.68614	4
10	1195.63173	598.31950	L	373.28093	187.14410	3
11	1308.71579	654.86153	L	260.19687	130.60207	2
12			K	147.11280	74.06004	1

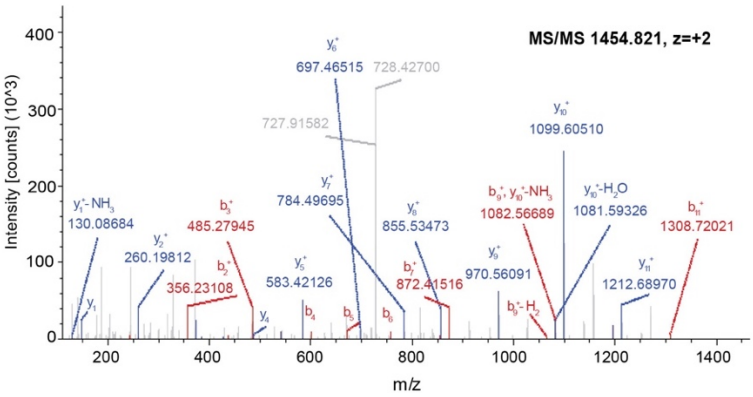

Fig. S5. Representative annotated MS/MS spectra and their fragmentation table of the ubiquitinated MK2 peptides identified. The peptide sequence, mass (m) and the charge (z) of each precursor peptide ion are indicated. The ubiquitinated lysine is referred as K-GG in the tables.

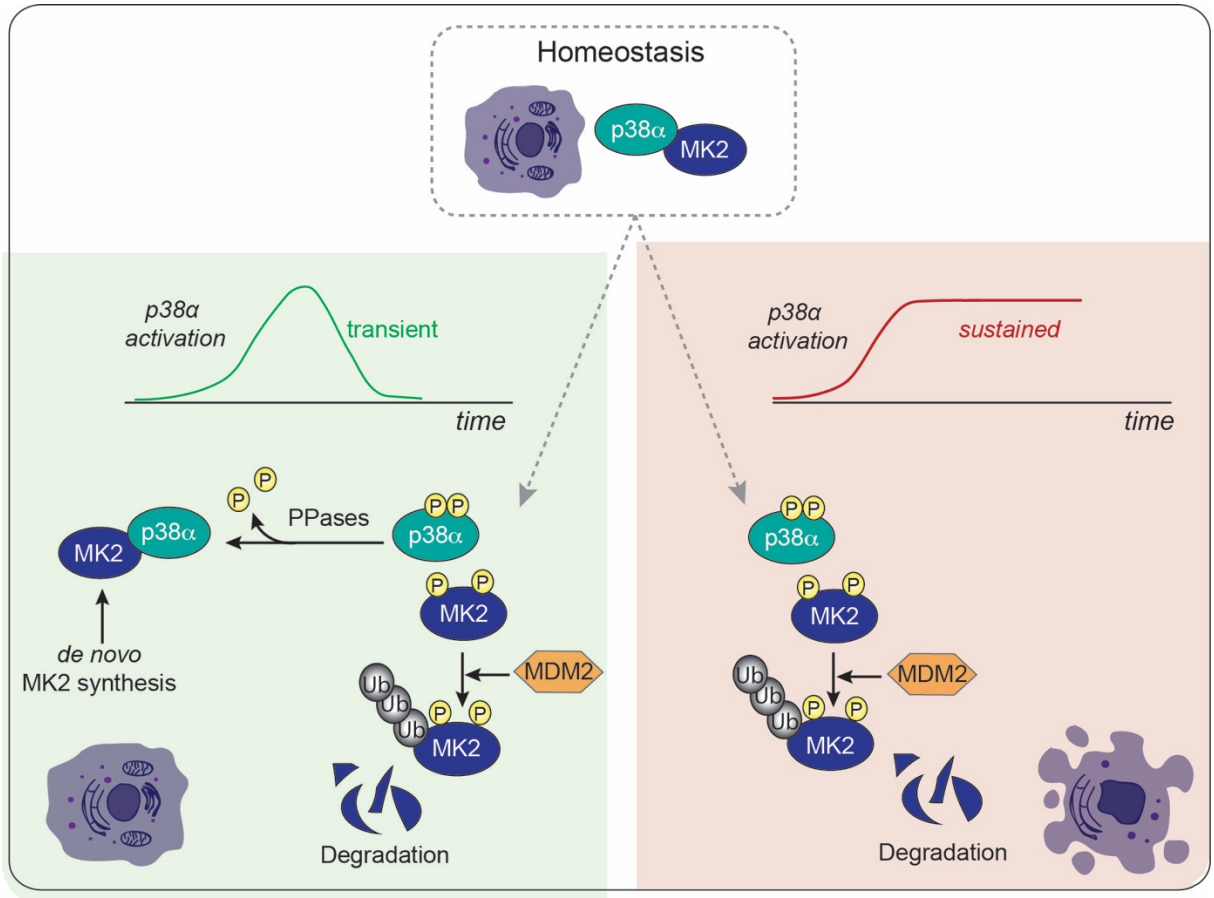

Fig S6. Regulation of the p38α-MK2 complex in response to different stimuli. In homeostasis, p38α and MK2 proteins form a complex. In response to stimuli that induce transient p38α activation (Left), both p38α and MK2 become phosphorylated and separate from each other, leading to MK2 ubiquitination by MDM2 and degradation by the proteasome. At later times, MK2 is re-expressed, p38α is dephosphorylated by phosphatases and they form a complex again. This regulatory feedback-loop allows the recovery of the stand-by cellular status. In contrast, severe stress induces persistent p38α activation (Right), which results in sustained phosphorylation of both p38α and MK2, precluding complex formation. Then MK2 is irreversibly degraded and its pro-survival function is lost leading to cell death.

Table S1. p38α mutants

Name	*Mutation*	*Reference*
CD	D313/315/316N	(7)
ED	E160/E161T	(8)
IA	I116A	(9)
DF	D176A/F327S	(10)
DG	D145G	(11)
KM, TY	K53M, T180A/Y182F	(12)

References

1. B. Canovas *et al.*, Targeting p38alpha Increases DNA Damage, Chromosome Instability, and the Anti-tumoral Response to Taxanes in Breast Cancer Cells. *Cancer Cell* **33**, 1094-1110 e1098 (2018).
2. C. Youssif *et al.*, Myeloid p38alpha signaling promotes intestinal IGF-1 production and inflammation-associated tumorigenesis. *EMBO Mol Med* **10**, e8403 (2018).
3. M. Soleimani, S. Nadri, A protocol for isolation and culture of mesenchymal stem cells from mouse bone marrow. *Nat Protoc* **4**, 102-106 (2009).
4. A. Kotlyarov *et al.*, MAPKAP kinase 2 is essential for LPS-induced TNF-α biosynthesis. *Nat Cell Biol* **1**, 94-97 (1999).
5. S. Regot, Jacob J. Hughey, Bryce T. Bajar, S. Carrasco, Markus W. Covert, High-Sensitivity Measurements of Multiple Kinase Activities in Live Single Cells. *Cell* **157**, 1724-1734 (2014).
6. D. G. Gibson *et al.*, Enzymatic assembly of DNA molecules up to several hundred kilobases. *Nat Methods* **6**, 343-345 (2009).
7. T. Tanoue, M. Adachi, T. Moriguchi, E. Nishida, A conserved docking motif in MAP kinases common to substrates, activators and regulators. *Nat Cell Biol* **2**, 110-116 (2000).
8. T. Tanoue, R. Maeda, M. Adachi, E. Nishida, Identification of a docking groove on ERK and p38 MAP kinases that regulates the specificity of docking interactions. *EMBO J* **20**, 466-479 (2001).
9. C. I. Chang, B. E. Xu, R. Akella, M. H. Cobb, E. J. Goldsmith, Crystal structures of MAP kinase p38 complexed to the docking sites on its nuclear substrate MEF2A and activator MKK3b. *Mol Cell* **9**, 1241-1249 (2002).
10. R. Diskin, N. Askari, R. Capone, D. Engelberg, O. Livnah, Active mutants of the human p38alpha mitogen-activated protein kinase. *J Biol Chem* **279**, 47040-47049 (2004).
11. Q. Li *et al.*, Determinants that control the distinct subcellular localization of p38alpha-PRAK and p38beta-PRAK complexes. *J Biol Chem* **283**, 11014-11023 (2008).
12. P. R. Mittelstadt, H. Yamaguchi, E. Appella, J. D. Ashwell, T cell receptor-mediated activation of p38{alpha} by mono-phosphorylation of the activation loop results in altered substrate specificity. *J Biol Chem* **284**, 15469-15474 (2009).